

2013

Examination Of Thermal Properties Of Carbon-Carbon And Graphitized Carbon-Carbon Composites

Melanie Jene' Patrick

North Carolina Agricultural and Technical State University

Follow this and additional works at: <https://digital.library.ncat.edu/theses>



Part of the [Mechanical Engineering Commons](#)

Recommended Citation

Patrick, Melanie Jene', "Examination Of Thermal Properties Of Carbon-Carbon And Graphitized Carbon-Carbon Composites" (2013). *Theses*. 319.

<https://digital.library.ncat.edu/theses/319>

This Thesis is brought to you for free and open access by the Electronic Theses and Dissertations at Aggie Digital Collections and Scholarship. It has been accepted for inclusion in Theses by an authorized administrator of Aggie Digital Collections and Scholarship. For more information, please contact iyanna@ncat.edu.

Examination of Thermal Properties of Carbon-Carbon and
Graphitized Carbon-Carbon Composites

Melanie Jené Patrick

A thesis submitted to the graduate faculty
in partial fulfillment of the requirements for the degree of
MASTER OF SCIENCE

Department: Mechanical Engineering
Major: Mechanical Engineering
Major Professor: Dr. Messiha Saad

North Carolina A&T State University
Greensboro, North Carolina
2013

School of Graduate Studies
North Carolina Agricultural and Technical State University

This is to certify that the Master's Thesis of

Melanie Jené Patrick

has met the thesis requirements of
North Carolina Agricultural and Technical State University

Greensboro, North Carolina
2013

Approved by:

Dr. Messiha Saad
Major Professor

Dr. Devdas Pai
Committee Member

Dr. Dhananjay Kumar
Committee Member

Dr. Samuel Owusu-Ofori
Department Chairperson

Dr. Sanjiv Sarin
Dean, The Graduate School

© Copyright by
Melanie Jené Patrick
2013

Biographical Sketch

Melanie Jené Patrick was born on June 28, 1989 to Gordon and Deborah Patrick in Washington, DC. She was raised in Mitchellville, MD and attended Clinton Christian School and Riverdale Baptist for elementary and middle school, respectively. Her love and interest for math and science led her to test for and enroll into the Science and Technology Program. While in the Science and Technology Program at Charles H. Flowers High School she was introduced to the field of engineering. Enjoying the statics and structures course she decided to complete her senior internship requirement in the Materials Science and Engineering Department at the University of Maryland College Park. There she worked immensely with the fabrication of functionally graded materials and developed a passion for composite materials. Initially, she believed that the enjoyment she received from working on this research and her intrigue with STEM (Science, Technology, Engineering, and Math) would be a good motivation to major in Materials Science and Engineering in college.

After working with her mentor in the internship program at the University of Maryland and talking with her teacher and mentor Mrs. Victoria Lee, she decided that Mechanical Engineering would be a better major to select. This field would give her the flexibility to attend a wider range of Universities as well as offer a broader course of study. An extensive curriculum would expose her to more skills and methodologies while still allowing her to gain a deeper understanding of and conduct research on composite materials.

She attended North Carolina Agricultural and Technical State University and earned her Bachelor of Science degree in Mechanical Engineering in May of 2011. In that same year she passed the exam to become a certified Engineer-In-Training in North Carolina. Melanie is now a candidate for the Master Science degree in Mechanical Engineering.

Dedication

To my parents I am eternally grateful and thankful for all of your encouragement, love, and support. To my family I thank you for always believing in me. To my friends I appreciate you being there to help me have a great balance of school, work, and fun.

Acknowledgements

I would like to extend my sincerest appreciation to Dr. Messiha Saad for being an informative and supportive advisor. This thesis would not have been possible without his guidance and him allowing me to conduct research in his Thermal Characterization Laboratory. I would also like to acknowledge the NASA-URC- Center for Aviation Safety (CAS) (Grant #NNX09AV08A) and the Oak Ridge National Laboratory's High Temperature Materials Laboratory (HTML) sponsored by the U.S. Department of Energy, Office of Energy Efficiency and Renewable Energy, Vehicle Technologies Program. Additionally, I would like to thank Dr. Shivakumar and the Center for Composite Materials Research (CCMR) at North Carolina A&T State University for providing an assistantship and sample materials for testing.

Moreover it is important that I recognize Dr. Devdas Pai and Dr. Dhananjay Kumar for their impeccable instruction and the knowledge I received in their courses as well as for them agreeing to serve on my thesis committee. Additionally, I would like to thank Matthew Sharpe for his assistance with the test sample preparation.

Table of Contents

List of Figures	viii
List of Tables	x
Nomenclature	xi
Abstract	2
CHAPTER 1 Introduction.....	3
1.1 Background	3
1.2 Objective	5
CHAPTER 2 Literature Review	7
2.1 Heat Conduction and Thermal Property Definitions	7
2.2 Theoretical Methods for Determining Thermal Conductivity of Composites.....	8
2.3 Experimental Methods for Determining Thermal Diffusivity of Composites.....	10
CHAPTER 3 Methodology.....	15
3.1 Thermal Diffusivity – The Flash Method	15
3.2 Specific Heat – Differential Scanning Calorimetry	20
3.3 Thermal Conductivity	22
CHAPTER 4 Experimental Technique	24
4.1 The Flash Method – Thermal Diffusivity Measurement	24
4.1.1 Experimental Apparatus.....	24
4.1.2 Test Specimen Preparation.	26
4.1.3 Experimental Procedure.....	27

4.2	Differential Scanning Calorimetry (DSC) – Specific Heat Measurement.....	28
4.2.1	Experimental Apparatus.....	28
4.2.2	Test Specimen Preparation.	30
4.2.3	Experimental Procedure.....	32
CHAPTER 5	Results.....	35
5.1	Thermal Diffusivity	35
5.2	Specific Heat.....	49
5.3	Thermal Conductivity	51
CHAPTER 6	Discussion and Future Research.....	54
6.1	Discussion	54
6.2	Future Research	54
References	56
<i>Appendix</i>	61

List of Figures

Figure 2.1. Thermal Wave Interferometry Experimental Set-up.....	11
Figure 2.2. Experimental Set-up of the Thermographic Method for In-Plane Measurement.	12
Figure 3.1. Schematic of the Flash Method.	16
Figure 3.2. Flash Method Thermogram.	18
Figure 4.1. Flash Line TM 2000 Thermal Properties Analyzer and Data Acquisition System.	24
Figure 4.2. Schematic of Bulk Carbon-Carbon with Cylindrical Specimens.	26
Figure 4.3. Cross-Section Schematic of the DSC.	29
Figure 4.4. Differential Scanning Calorimeter – DSC 200 F3 Maia®.	30
Figure 4.5. DSC Test Specimen Inside Open Aluminum Crucible with Lid.	31
Figure 4.6. Crucibles Centered on the Heat Flux Sensors.	33
Figure 5.1. Published and Experimental Thermal Diffusivity Data of Thermographite.	35
Figure 5.2. Through-The-Thickness Thermal Diffusivity of Carbon-Carbon (1K).	36
Figure 5.3. Through-The-Thickness Thermal Diffusivity of Graphitized Carbon-Carbon (1K).	37
Figure 5.4. Comparison of Through-The-Thickness Thermal Diffusivity of Carbon-Carbon.	38
Figure 5.5. Through-The-Thickness Thermal Diffusivity of Carbon-Carbon (3K).	39
Figure 5.6. In-Plane Thermal Diffusivity of Carbon-Carbon (3K).....	40
Figure 5.7. In-Plane and Through-The-Thickness Thermal Diffusivity of Carbon-Carbon (3K).	40
Figure 5.8. Effect of Coating on In-Plane Thermal Diffusivity of Carbon-Carbon.	41
Figure 5.9. Coating Effect on Through-The-Thickness Thermal Diffusivity of Carbon-Carbon.	42
Figure 5.10. Half-Times of Tested Materials Compared to Allowable Limits.....	46
Figure 5.11. Comparison of the Carbon-Carbon Thermograms to the Theoretical Model.	47
Figure 5.12. Rear Face Temperature Rise: Mathematical Model versus Experimental Result.	47

Figure 5.13. Graphitized Carbon-Carbon Thermograms Versus the Theoretical Model.	48
Figure 5.14. Carbon-Carbon (3K) Thermograms Versus the Theoretical Model.....	49
Figure 5.15. Specific Heat of Carbon-Carbon Versus Poco-Graphite.....	50
Figure 5.16. Specific Heat of Tested Materials.	51
Figure 5.17. Thermal Conductivity Comparison of Carbon-Carbon (1K).	52
Figure 5.18. Thermal Conductivity of In-Plane and Through-The-Thickness Carbon-Carbon. ..	53

List of Tables

Table 1.1 Tested Materials Specifications	6
Table 4.1 Average Specifications of Flash Method Test Specimens.....	27
Table 4.2 Typical Dimensions of DSC Test Specimens.....	31
Table 5.1 Thermal Diffusivity Results for Carbon-Carbon (1K-ttt).....	43
Table 5.2 Thermal Diffusivity Results for Graphitized Carbon-Carbon (1K-ttt).....	44
Table 5.3 Thermal Diffusivity Results for Carbon-Carbon (3K-ttt).....	44
Table 5.4 Thermal Diffusivity Results for Carbon-Carbon (3K-ip).....	45
Table 5.5 Thermal Property Results at Room Temperature	53

Nomenclature

A	cross-sectional area
\bar{a}	measurement mean
a_i	i^{th} measurement of the sample
c_p	specific heat (J/kg·K)
e	margin of error
E	calibration constant
g	depth (m)
h	specific enthalpy (J/kg)
H	enthalpy (J)
i-p	In-Plane
k	thermal conductivity (W/m·K)
K	thousands of filaments per fiber strand
K_R	correction factor
L	sample thickness (cm)
m	mass (kg)
n	number of iterations
N	number of measurements
q	rate of heat conducted per unit volume (W/m ³)
\dot{Q}	rate of heat flow (W)
Q	pulse of radiant energy, heat (J/ cm ²)
s_x	sample standard deviation
SE	standard deviation on the mean

t	time (s)
T	temperature (K)
t-t-t	Through-The-Thickness
V	dimensionless quantity
x	distance (m)

Greek Symbols

α	thermal diffusivity (cm ² /s)
Δ	differential quantity
ρ	density (kg/m ³)
σ	standard deviation
ω	dimensionless quantity

Subscripts

ref	reference
0	initial time step
$\frac{1}{2}$	half
1C	in-plane composite property
2C	through-the-thickness composite property
1f	in-plane fiber property
2f	through-the-thickness fiber property
F	final time
f	fiber
m	matrix

Abstract

Thermal characterization of composites is essential for their proper assignment to a specific application. Specific heat, thermal diffusivity, and thermal conductivity of carbon-carbon composites are essential in the engineering design process and in the analysis of aerospace vehicles, space systems and other high temperature thermal systems. Specifically, thermal conductivity determines the working temperature levels of a material and is influential in its performance in high temperature applications.

There is insufficient thermal property data for carbon-carbon composites over a range of temperatures. The purpose of this research is to develop a thermal properties database for carbon-carbon composites that will contain in-plane (i-p) and through-the-thickness (t-t) thermal data at different temperatures as well as display the effects of graphitization on the composite material. The carbon-carbon composites tested were fabricated by the Resin Transfer Molding (RTM) technique, utilizing T300 2-D carbon fabric and Primaset PT-30 cyanate ester resin.

Experimental methods were employed to measure the thermal properties. Following the ASTM standard E-1461, the flash method enabled the direct measurement of thermal diffusivity. Additionally, differential scanning calorimetry was performed in accordance with the ASTM E-1269 standard to measure the specific heat. The measured thermal diffusivity, specific heat, and density data were used to compute the thermal conductivity of the carbon-carbon composites. The measured through-the-thickness thermal conductivity values of all the materials tested range from 1.0 to 17 W/m·K, while in-plane values range from 3.8 to 4.6 W/m·K due to the effect of fiber orientation. Additionally, the graphitized samples exhibit a higher thermal conductivity because of the nature of the ordered graphite structure.

CHAPTER 1

Introduction

1.1 Background

Advances in innovation in today's technologies has allowed for the accomplishment of once thought inconceivable tasks. Miniaturization of electronics, faster heat dissipation for space vehicle components, and more efficient aircrafts of lighter components are just some of the developments. With these improvements there is an increased need for materials that can achieve and withstand the desired extreme conditions. A composite is a material system consisting of two or more phases on a macroscopic scale whose properties are designed to be superior to those of the constituent materials acting independently. The reinforcement phase is usually discontinuous and stronger, and the matrix phase is weaker and continuous (Daniel & Ishai, 2006). Composite materials are often sought as the answers to these problems because they combine the beneficial qualities of the constituent materials and exhibit improved performance.

Thermal and mechanical characterization of composite materials is the key for appropriate utilization. More often only mechanical properties of a composite are used to deem it suitable for an application, but adding a thermal aspect to this determination yields a stronger verification to the composite's applicability. Thermal diffusivity, specific heat, and thermal conductivity identify some of the crucial thermal properties. Specifically, thermal conductivity determines the working temperature levels of the material, and it plays a critical role in the performance of materials in high temperature applications such as aerospace vehicles and space systems. It is an essential parameter in problems involving heat transfer and thermal structures (Saad, Baker, & Reaves, 2011). There are several factors that influence thermophysical properties including but not limited to the fiber type, fiber alignment (Chen, Ren, Zhang, Zhang, & Wu, 2012), and

volume fraction of the constituent materials as well as the thermal processing technique used in fabrication (Ohlhorst, Vaughn, Ransone, & Tsou, 1997).

The carbon-carbon composites have superior thermal and mechanical characteristics. They are lightweight, retain their mechanical strength at high temperatures, possess a low coefficient of thermal expansion, and exhibit low wear from room temperature to high temperatures. Additionally, they have a high and tailorable thermal conductivity and can withstand temperatures in excess of 3300 K (Luo et al., 2004); (Grujicic et al., 2006). These characteristics make the carbon-carbon composites attractive candidates as advanced thermal system materials (Ohlhorst et al., 1997). Primarily, the composites are employed in the aerospace industry thereby capitalizing on their auspicious thermal capabilities. Due to their excellent mechanical, thermal, wear, and frictional properties the carbon-carbon composites are great candidates in today's brake industries in aviation and some automotive industries (Iqbal, Dinwiddie, Porter, Lance, & Filip, 2011). Also, these materials have densities much lower than those of metals and ceramics and hence make components of lower weights, an important consideration for aero-vehicles (Manocha, 2003). Applications requiring thermal management or system elements needing high temperature stability, including rocket nozzles and exit cones, also benefit from the desirable carbon-carbon composite qualities.

Graphitization of the carbon-carbon composite involves heat-treating it to a temperature of 2500°C and is an example of a technique that allows for the thermal conductivity to be altered. This processing technique extends the composite's capabilities and alters its molecular and thermal makeup. Increasing the graphite order of the standard carbon structure, results in a significantly higher thermal conductivity than the non-graphitized composite.

1.2 Objective

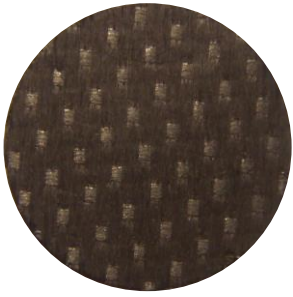



The overall goal of this research is to develop a thermal properties database for carbon-carbon and graphitized carbon materials. The through-the-thickness (t-t) and in-plane (i-p) thermal properties of the carbon-carbon composites and graphitized carbon-carbon composites were examined. The through-the-thickness measurements were conducted experimentally utilizing the flash method, an established technique defined by the ASTM E-1461 test standard. The in-plane testing was achieved experimentally in a similar fashion and the theoretical analysis was accomplished using the rule of mixtures. The specific heat of the material is independent of specimen orientation and was determined using the ASTM E-1269 test standard. This information along with density data allowed for the determination of thermal conductivity.

The materials tested were developed at Center for Composite Materials and analyzed in the Thermal Characterization Laboratory at North Carolina A&T State University as part of the NASA-URC “Center for Aviation Safety” sponsored research. All of the carbon-carbon composites were produced by the Resin Transfer Molding (RTM) process. The constituents are a plain weave T300 2-D carbon fabric and a Primaset PT-30 cyanate ester resin. The estimated fiber volume fraction is 55%. Four categories of the materials were prepared for analysis. One portion of the specimens had a 1K x 1K plain weave T300 fabric and were cut as t-t-t samples with no heat treatments. Several other specimens possessed a 1K x 1K plain weave T300 fabric and were cut as t-t-t samples with a graphitization heat treatment. The other of the carbon-carbon samples contained the 3K x 3K plain weave T300 fabric and were not heat treated. Some of these were cut to t-t-t samples and the others were prepared as i-p samples. The K term refers to 1,000 filaments in a strand, which describes the tow count of the fibers in the fabric. For instance the 3K x 3K plain weave fabric would indicate that the fabric contains 3,000 filaments in each strand

in both directions. Table 1.1 displays photos of the different categories of the materials with the associated orientation, tow count, and heat treatment.

Table 1.1

Tested Materials Specifications

Material	Orientation	Fiber Tow	Heat Treatment	PHOTO
Carbon-Carbon	t-t-t	1K x 1K	None	
Graphitized Carbon-Carbon	t-t-t	1K x 1K	Graphitized to 2500 °C	
Carbon-Carbon	t-t-t	3K x 3K	None	
Carbon-Carbon	i-p	3K x 3K	None	

CHAPTER 2

Literature Review

2.1 Heat Conduction and Thermal Property Definitions

Heat conduction is the transfer of energy from a region of high temperature to a region of low temperature via the interaction of adjacent molecules due to the existence of a temperature gradient with the system (Hahn & Özişik, 2012). The mathematical theory of heat conduction was developed by Joseph Fourier and his law describes, heat flux, the flow of heat per unit time. Fourier's law of Heat Conduction can be expressed in several ways. The rate of heat flow in one direction can be given as:

$$\dot{Q} = -kA \frac{dT}{dx} \quad (2.1)$$

where k is thermal conductivity, A is the cross sectional area, dT is temperature difference, and dx is the material thickness. If an energy balance is executed and there is constant thermal conductivity, a differential form in one dimension is delineated by (Hahn & Özişik, 2012):

$$\frac{1}{\alpha} \frac{\partial T}{\partial t} = \frac{\partial^2 T}{\partial x^2} + \frac{q}{k} \quad (2.2)$$

where q is the rate of heat conducted per unit volume in units W/m^3 , α is thermal diffusivity in m^2/s , and k is thermal conductivity in $\text{W}/\text{m}\cdot\text{K}$.

Thermal conductivity plays a major role in this this analysis because the flow of heat for a given temperature gradient is directly proportional to the thermal conductivity of the material (Hahn & Özişik, 2012). As defined by the Springer Handbook of Materials Measurement Methods, given two surfaces on either side of a material with a temperature difference between them, the thermal conductivity is the heat energy transferred per unit time and per unit surface area, divided by the temperature difference. Overall, thermal conductivity is a material's

capability to conduct energy, and in this research it is expressed in the SI units of W/m·K. Materials of high thermal conductivities transfer heat energy well and are considered as conductors. Materials that conduct heat poorly are deemed as insulators and have low thermal conductivity values.

Thermal diffusivity measures the speed of the propagation of heat into a material during changes of temperature. The higher the thermal diffusivity the faster the response of the material to thermal perturbations and the faster such changes propagate throughout the material (Hahn & Özişik, 2012). Materials of larger values of thermal diffusivity will transmit heat quickly and will adjust to the temperature of their surroundings quickly. On the other hand, substances of low thermal diffusivities will take a much longer time to conform to the temperature of their surroundings. Additionally, specific heat is the amount of heat, measured in calories, required to raise the temperature of one gram of a substance by one degree Celsius (Czichos, H., Saito, T., & Smith, L., 2006). These properties are related to thermal conductivity by the following equation:

$$\alpha = \frac{k}{\rho c_p} \quad (2.3)$$

where α is the thermal diffusivity, ρ is the density of the material and c_p is the specific heat.

2.2 Theoretical Methods for Determining Thermal Conductivity of Composites

The thermal conductivity of a composite can be predicted provided suitable assumptions are made about the flow of heat through the constituents. It is possible to measure or obtain the in-plane properties of the fiber and resin constituents of a composite. In general, the resin can be considered to have macroscopic isotropy (Takezawa, 2005) and therefore has the same properties in all directions. For the axial case, the thermal gradient is the same in each constituent and the thermal conductivity is given by a simple rule of mixtures (Hull & Clyne, 1996):

$$k_{1C} = V_f k_{1f} + V_m k_m \quad (2.4)$$

where k_{1C} is the in-plane thermal conductivity of the composite, V_f is the fiber volume fraction, k_{1f} is the in-plane thermal conductivity of the fiber, V_m is the matrix volume fraction, and k_m is the thermal conductivity of the matrix. In the scope of this research the carbon fabric is the fiber or reinforcement, and the cyanate ester resin is the matrix of the composite.

Predictions of the through-the-thickness thermal conductivity are challenging. There exists a range of theoretical approximations for this transverse property from simple models using combinations of thermal resistance to more sophisticated conduction models capable of accommodating interphase resistance. Measuring the matrix properties is usually direct since this material can be made in bulk form, but determining the fiber properties in the transverse direction is more difficult than the axial direction because of the small fiber size (Wetherhold & Wang, 1994). Because of the issues with direct measurement, it is common to evaluate the composite and matrix properties and then infer the fiber values using a model. Two of these models were investigated to evaluate their applicability to this research. A simple thermal resistance model is given by (Chawla, 1998):

$$k_{2C} = (1 - \sqrt{V_f})k_m + \frac{k_m \sqrt{V_f}}{1 - \sqrt{V_f} (1 - k_m/k_{2f})} \quad (2.5)$$

where k_{2C} is the transverse thermal conductivity of the composite and k_{2f} is the transverse thermal conductivity of the fiber. A model based on bounding principles and analogies to mechanical shear properties is expressed as (Hashin, 1983):

$$k_{2C} = k_m + \frac{V_f}{1/(k_{2f} - k_m) + (1 - V_f)/2k_m} \quad (2.6)$$

Using both of these theories Wetherhold and Wang were able to calculate the transverse thermal conductivity of the fiber and the resulting value was the same for both techniques.

Many models for predicting the transverse thermal conductivity of a composite work well and are robust if the fiber and matrix conductivities are similar (Wetherhold & Wang, 1994). In the research experiments and analyses referenced above the thermal conductivity values of the matrix and the fiber are of the same order of magnitude. This allows for calculations to be performed and reasonable results to be found. If the fiber conductivity substantially exceeds the matrix conductivity certain problems can arise (Wetherhold & Wang, 1994). In this research the thermal conductivity of the carbon fiber is an order of magnitude higher than that of the cyanate ester resin. Therefore this technique could not be applied to the composite materials used in this research.

2.3 Experimental Methods for Determining Thermal Diffusivity of Composites

Carbon composites are used in a wide variety of fields, and it is necessary to develop and retain a database of detailed thermal information about the material to ensure safe operating temperatures in factories and proper function in systems. Currently, there exists a number of research efforts to determine the mechanical properties but there is limited information on the thermal characterization of carbon-carbon. There is published information regarding different experimental methods used to determine thermal diffusivity to allow for the calculation of thermal conductivity. Iqbal *et al.* (2011) investigated the effect of heat treatment on thermal properties of carbon-carbon composites and Ohlhorst *et al.* (1997) generated a thermal conductivity database of selected carbon-carbon and graphitized carbon-carbon materials.

The thermal diffusivity of a material can be measured in several different ways. Available techniques include Thermal wave Interferometry (TWI), Thermographic methods, the flash

method, and others. The most common of these is the flash method. This technique is so widely accepted that many countries consider it a standard. Specifically, it is defined by the American Society for Testing and Materials Standard E-1461 and has the versatility of using a lamp or laser as the energy source. The two less popular techniques will be briefly described here and a detailed explanation of the flash method will be given later.

Thermal wave interferometry (TWI) is used to measure the thermal diffusivity of coatings and thin slabs (Cernuschi et al., 2002). The method is able to successfully conduct measurements based on the fact that thermal waves with specific angular frequencies will propagate through layers of a material in a certain way. The waves are reflected and transmitted at the separation surface of the two different materials like conventional waves. The interference between propagating and reflected waves alters the phase and the amplitude of the AC component of the surface temperature (Cernuschi et al., 2002). The schematic is displayed in Figure 2.1 (Cernuschi et al., 2002). This method is somewhat complex due to its involvement of multiple waves of different frequencies. In comparison to the flash method it is not widely used.

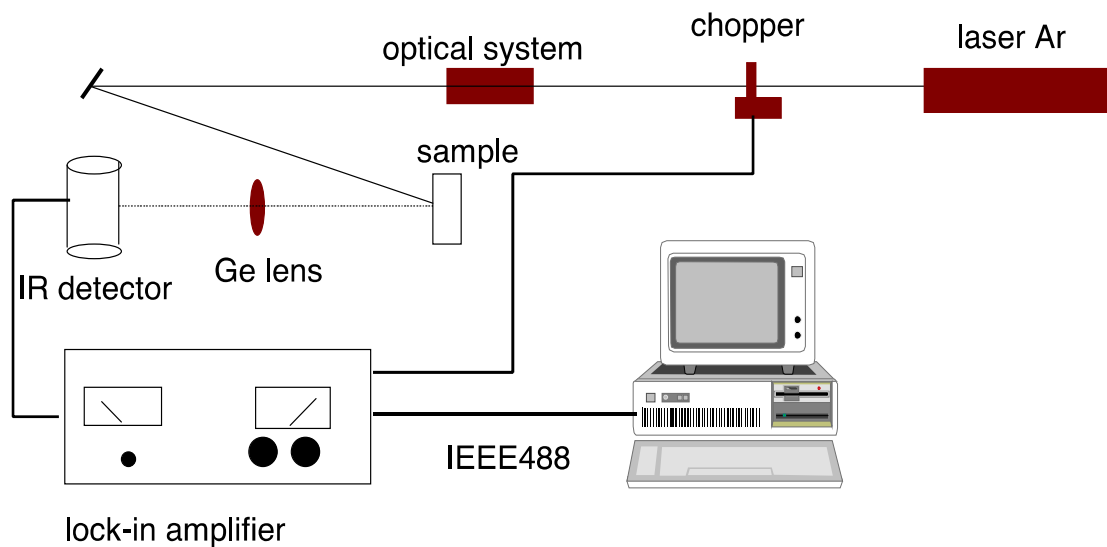


Figure 2.1. Thermal Wave Interferometry Experimental Set-up.

The thermographic method is based on the temperature on the rear surface of an infinite slab that has been instantaneously heated by a Gaussian shaped source. The temperature distribution analysis of this method assumes an infinite test specimen. This technique is used for the measurement of the in-plane thermal diffusivity, and the experiment is performed on a specimen with a much larger diameter in comparison to the flash method (Cernuschi, Bison, Figari, Marinetti, & Grinzato, 2004). A schematic of the thermographic method for the in-plane measurement is given in Figure 2.2 (Cernuschi et al., 2002).

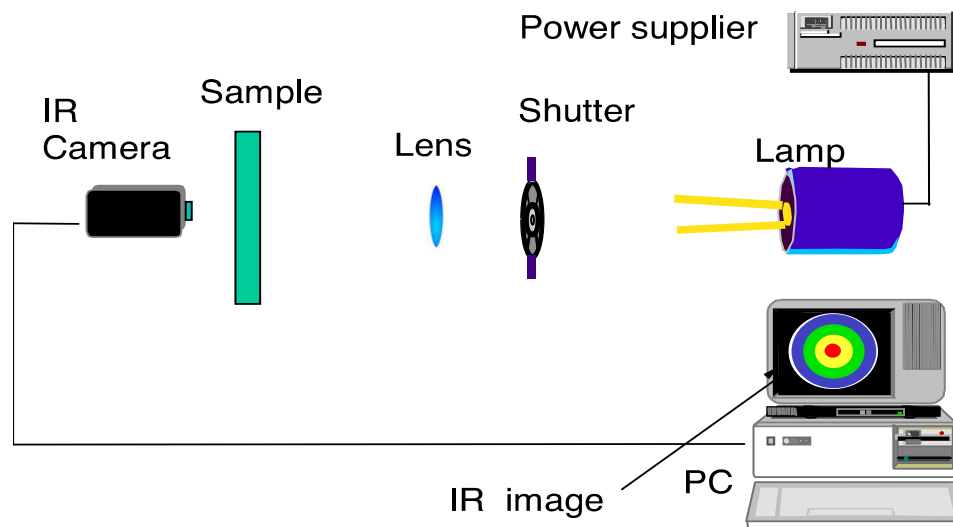


Figure 2.2. Experimental Set-up of the Thermographic Method for In-Plane Measurement.

The investigation conducted by Iqbal *et al.* (2011) includes the effect of heat treatment on the through-the-thickness thermal properties of two directional (2D) pitch-based carbon fiber, and three dimensional (3D) Polyacrylonitrile (PAN) based carbon fiber carbon-carbon composites. The samples were heat treated at 1800°C, 2100°C and 2400°C, and the thermal diffusivity, specific heat, and thermal conductivity were measured in accordance to the ASTM C1470 standard. When analyzing the thermal conductivity of the non-heat treated samples it was found that these specimens displayed the lowest thermal conductivity and the values decreased

exponentially as temperature increased (Iqbal et al., 2011). Additionally, the thermal conductivity increases substantially with heat treatment temperature. The increase in thermal conductivity is due to the increase in crystallinity of the heat-treated materials when compared to the non-heat treated material. In general, thermal conductivity of the carbon fiber carbon-carbon composites increased with heat treatment temperature, making it appear that high heat treatment has a beneficial effect on materials (Iqbal et al., 2011).

Ohlhorst *et al.* (1997) recognizes that carbon-carbon composite materials possess characteristics that make them exceptional materials in the construction of advanced thermal protection systems. In order for the designers of these thermal systems to appropriately assign materials it is necessary that information about the constituent materials, fabrication technique, and thermophysical properties of the composites be known. To contribute to this need Ohlhorst *et al.* (1997) attempts to compile a consistent set of in-plane and through-the-thickness thermal conductivity values from room temperature to 1922 K for carbon-carbon composites. The materials were composed of a variety of combinations of fiber types and resins including but not limited to Amoco T-300 fiber, Amoco T-50 fiber, phenolic resin, and chemical vapor infiltration (CVI) deposited pyrolytic carbon. The different composite configurations were heat treated at temperatures ranging from 1173 K to 2423 K. The thermal diffusivity measurements were conducted using the flash diffusivity method. The through-the-thickness direction measurements were achieved using the traditional round specimens, while the in-plane measurements utilized square specimens.

For materials that were heat treated in the range given previously and that possessed a maximum fabrication temperature of 2373 K or below, the maximum in-plane thermal conductivity values were from 20 to 68 W/m·K. In contrast, the through-the-thickness thermal

conductivity values of these materials were much lower ranging from 3 to 12 W/m·K (Ohlhorst et al., 1997). These results are in concurrence with conclusions found in many other studies that the in-plane thermal conductivity values of composite materials are greater than the through-the-thickness values because of fiber orientation distribution on thermal properties (Mutnuri, 2006); (Iqbal et al., 2011); (Klett & Conway); (Adams, Katzman, Rellick, & Stupian, 1998). Though a significant amount of thermal property data was given in this research, no non-heat treated samples were investigated.

CHAPTER 3

Methodology

3.1 Thermal Diffusivity – The Flash Method

Thermal diffusivity measures how quickly heat can travel through a material. It determines the working temperature levels of the material and plays a critical role in the performance of materials in high temperature applications. It is an important property required in purposes where there are transient heat flow conditions. Some of these include the design of thermal systems, determination of safe operating temperature, process control, and quality assurance (ASTM Standard E-1461, 2007). The thermal diffusivity of a material can be measured in several different ways. There are steady-state methods as well as transient techniques. Available procedures include Thermal Wave Interferometry (TWI), Thermographic methods, the flash method, the Hot-wire method, and others (Patrick & Saad, 2012). Recently, transient techniques have been preferred in measuring thermal properties of materials, the most common of these being the flash method (Nunes dos Santos, 2007).

W. J. Parker founded the flash method in 1961, and it is the most frequently used transient photothermal technique and has the versatility of using a lamp or laser as the energy source. In many countries it is considered a standard for thermal diffusivity measurement of solid materials (Cernuschi et al., 2004). This method is highly regarded owing to the small test specimen, rapid measurement speed, and high precision (Wei, 1989). As adopted by the United States, the laser flash method is a standard test method and is defined by the American Society for Testing and Materials standard E-1461. It involves a small cylindrical, thin disk specimen being heated in a closed environment to a desired temperature, usually between 20 and 500°C. Once the disk and the environment have reached the specified temperature, the front face is

subjected to quick radiant energy pulse as shown in Figure 3.1. The energy source can be a laser or a lamp. The front face absorbs the energy pulse, and a detector measures the resulting temperature change with respect to time on the rear face of the sample. The data acquisition system then records the temperature change of the rear face of the specimen versus time. In general, the thermal diffusivity value is calculated from the specimen thickness and the time required for the rear face temperature rise to reach certain percentages of its maximum value (ASTM Standard E-1461, 2007). A graphical representation of this data is called the thermogram of the flash. Figure 3.2 displays the theoretical model thermogram. The time in which it takes the rear face of the specimen to reach half the maximum temperature rise is called the halftime, $t_{1/2}$.

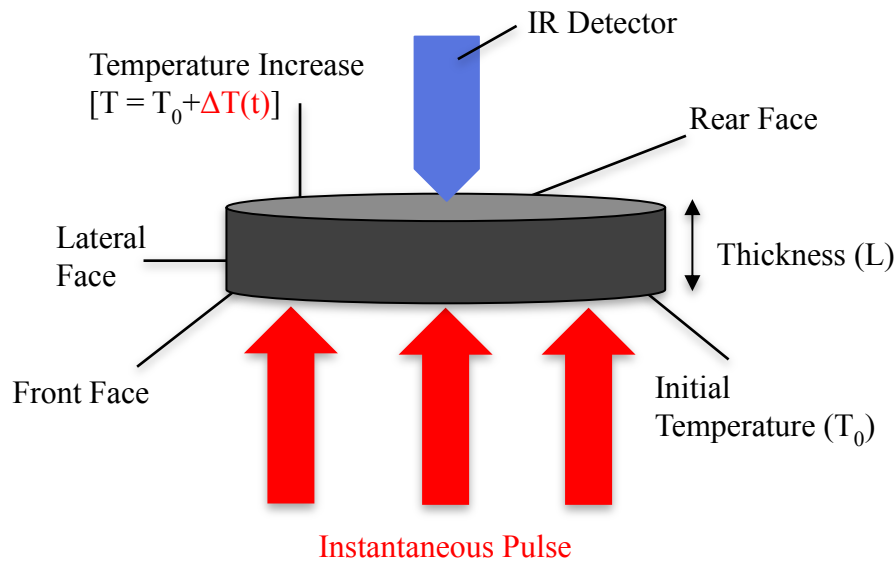


Figure 3.1. Schematic of the Flash Method.

Utilizing the equation for the temperature distribution within a thermally insulated solid of uniform thickness, L , developed by Carslaw and Jeager (1959), a mathematical expression to calculate thermal diffusivity was derived (Parker, Jenkins, Butler, & Abbott, 1961). An abbreviated version of this derivation is given as (refer to Appendix for complete derivation):

$$T(x, t) = \frac{1}{L} \int_0^L T(x, 0) dx + \frac{2}{L} \sum_{n=1}^{\infty} \exp\left(\frac{-n^2 \pi^2 \alpha t}{L^2}\right) \cos \frac{n\pi x}{L} \int_0^L T(x, 0) \cos \frac{n\pi x}{L} dx \quad (3.1)$$

where α is the thermal diffusivity in cm^2/s . If a pulse of radiant energy, Q (J/cm^2), is instantaneously and uniformly absorbed into a small depth referred to as g , at the front face ($x=0$) of the thermally insulated solid material (Clark & Taylor, 1975), the temperature distribution at the initial condition is given by:

$$T(x, 0) = \frac{Q}{\rho C_p g} \quad \text{for } 0 < x < g \quad (3.2)$$

$$T(x, 0) = 0 \quad \text{for } g < x < L \quad (3.3)$$

where ρ is the density and c_p is the specific heat capacity of the material. With the above initial conditions, equation 3.1 can be expressed as:

$$T(x, t) = \frac{1}{L} \left[\int_0^g \frac{Q}{\rho C_p g} dx + \int_g^L 0 \cdot dx \right] + \frac{2}{L} \sum_{n=1}^{\infty} \exp\left(\frac{-n^2 \pi^2 \alpha t}{L^2}\right) \cos \frac{n\pi x}{L} \left[\int_0^g \frac{Q}{\rho C_p g} \cos \frac{n\pi x}{L} dx + \int_g^L 0 \cdot \cos \frac{n\pi x}{L} dx \right] \quad (3.4)$$

After integration equation 3.4 can be written as:

$$T(x, 0) = \frac{Q}{\rho C_p L} \left[1 + 2 \sum_{n=1}^{\infty} \exp\left(\frac{-n^2 \pi^2 \alpha t}{L^2}\right) \cos \frac{n\pi x}{L} \cdot \frac{\sin \frac{n\pi g}{L}}{\frac{n\pi g}{L}} \right] \quad (3.5)$$

For materials that are opaque to the energy pulse, the adsorption depth, g , is a very small number. It then it follows that

$$\sin \frac{n\pi g}{L} \cong \frac{n\pi g}{L} \quad (3.6)$$

$$\cos \frac{n\pi g}{L} = (-1)^n \quad (3.7)$$

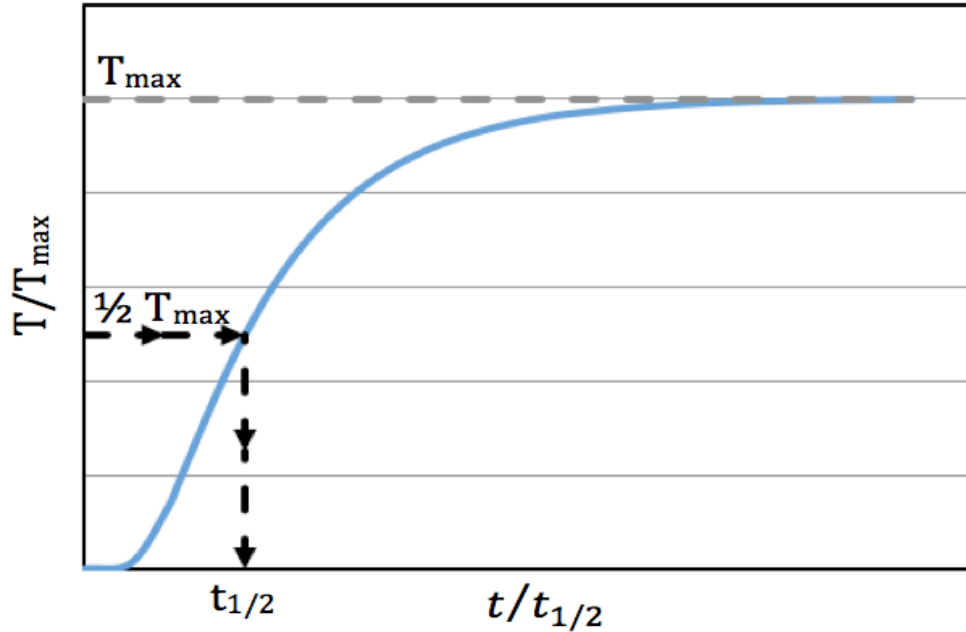


Figure 3.2. Flash Method Thermogram.

Once these are applied, the temperature distribution at the rear face ($x=L$) is expressed as (Parker et al., 1961):

$$T(L, t) = \frac{Q}{\rho C_p L} \left[1 + 2 \sum_{n=1}^{\infty} (-1)^n \exp\left(\frac{-n^2 \pi^2}{L^2} \alpha t\right) \right] \quad (3.8)$$

Setting

$$T_m = \frac{Q}{\rho C_p L} \quad (3.9)$$

where T_m is the maximum temperature at the rear face, (Parker et al., 1961) then defined two dimensionless parameters, V and ω as:

$$V(L, t) = \frac{T(L, t)}{T_m} \quad (3.10)$$

$$\omega = \frac{\pi^2 \alpha t}{L^2} \quad (3.11)$$

Combining equations 3.8, 3.10, and 3.11 yields (Parker et al., 1961):

$$V = 1 + 2 \sum_{n=1}^{\infty} (-1)^n \exp(-n^2 \cdot \omega) \quad (3.12)$$

Setting $V = 0.5$ allows for the determination of ω at the time required for the rear face to reach half of the maximum temperature rise. Substituting $\omega = 1.36975$ into equation 3.11 allows for a mathematical equation for thermal diffusivity to be stated as (Parker et al., 1961):

$$\alpha = 0.138785 \frac{L^2}{t_{1/2}} \quad (3.13)$$

W. J. Parker's derivation is a theoretical model of the flash method and is the ideal case. It assumes that the specimen is mostly homogeneous and isotropic, that there is one dimensional heat flow, that there are no heat losses from the specimen, and that the absorption of the pulse energy into the specimen is in a very thin layer (ASTM Standard E-1461, 2007). It also assumes that energy pulse is uniformly subjected across the front face of the specimen and that the pulse is instantaneous. Because of this, since Parker's original derivation, many researchers have developed correction factors. These include but are not limited to Cowan, Clark and Taylor, Koski, and Heckman (Beck & Dinwiddie, 1995). Each of these correction factors use different or a combination of methods to reanalyze the theoretical model and impose additional parameters. Some of these correction factors account for finite pulse time effect, but the pulse duration in this research can be considered infinitesimally short due to the use of a commercial apparatus, where the pulse energy absorption at the front face of the sample can be assumed uniform. The Clark and Taylor (1975) correction factor accounts for radiation heat losses and is used in the research. This correction factor was deemed suitable for implementation in this research because radiation heat loss is apparent in this experiment. In addition, Clark and Taylor examined the thermogram at different points before the maximum temperature rise was reached and developed a correction factor. The correction factor is computed using the following equation:

$$K_R = -0.3461467 + 0.361578 \left(\frac{t_{0.75}}{t_{0.25}} \right) - 0.06520543 \left(\frac{t_{0.75}}{t_{0.25}} \right)^2 \quad (3.14)$$

Specifically, they analyzed the time to reach 25 percent and 75 percent of the maximum temperature change. The corrected thermal diffusivity equation as defined by Clark and Taylor is

$$\alpha_{corrected} = \frac{\alpha K_R}{0.138785} \quad (3.15)$$

3.2 Specific Heat – Differential Scanning Calorimetry

Specific heat signifies how much heat per unit mass is required to raise the temperature of a material one degree Celsius. Differential Scanning Calorimetry (DSC) is a common technique used to measure the specific heat of materials. This technique is based upon the measurement of the change of the difference in the heat flow of the unknown material to that of a reference sample, while they are being subjected to a controlled temperature sequence (Höhne, Hemminger, & Flammersheim, 2003). Utilizing the measured heat flow rate of the unknown sample, Differential Scanning Calorimetry can determine how a material's heat capacity varies with respect to temperature.

Differential scanning calorimetry (DSC) is a thermo-analytical technique that is widely used for the measurement of specific heat. As accepted by the United States, its methodology is defined by ASTM standard E-1269. To conduct a differential scanning calorimetry measurement, a test specimen and reference sample are placed on a metallic block with high thermal conductivity and are enclosed in a furnace within the calorimeter. The metallic block ensures a good heat-flow path between the specimen and reference. The sample and the reference are subjected to an identical temperature program. The heat capacity changes in the specimen, which leads to a difference of temperature and heat flux relative to the reference. The calorimeter measures the temperature difference and calculates heat flow from calibration data.

As a result, the specific heat of the sample can be calculated using the heat flow results. To calculate the specific heat of an unknown material, the heat flux of the unknown and a reference must be measured using the differential scanning calorimeter. Using the measured heat flux values and the known specific heat of the reference, the specific heat of the unknown material can be calculated using the ratio method technique. Since the differential scanning calorimeter is at constant pressure, the change in enthalpy of the reference is equal to the heat absorbed or released by the reference (ASTM Standard E-1269, 2005). This is depicted mathematically as:

$$Q = m \cdot dh \quad (3.16)$$

Dividing both sides of the above equation by time leads to the following relationship:

$$\dot{Q} = m \frac{dh}{dt} = m \frac{dq}{dt} \quad (3.17)$$

where dq/dt is the heat rate and dh/dt is the change of enthalpy with respect to time. At constant pressure, the relationship for specific heat can be written as:

$$c_p = \left(\frac{1}{m}\right) \frac{dH}{dT} \quad (3.18)$$

where

$$dH = m \cdot dh \quad (3.19)$$

Using the chain rule the equation can be rewritten as:

$$c_p = \left(\frac{1}{m}\right) \frac{dt}{dT} \frac{dH}{dt} \quad (3.20)$$

From equations 3.17 and 3.20, the specific heat can be written as:

$$c_p = E \left(\frac{1}{m} \right) \left[\left(\frac{dt}{dT} \right) \left(\frac{dQ}{dt} \right) \right] \quad (3.21)$$

where E is the calibration constant and dt/dT is the inverse temperature distribution over time.

Using the ratio method, equation 3.21 can be written for the reference material as:

$$c_{p_{ref}} = E \left[\left(\frac{1}{m_{ref}} \right) \left(\frac{dt}{dT} \right) \left(\frac{dQ}{dt} \right)_{ref} \right] \quad (3.22)$$

Rearranging, the calibration constant can be expressed by:

$$E = \frac{C_{p_{ref}} m_{ref}}{\left(\frac{dt}{dT} \right) \left(\frac{dQ}{dt} \right)_{ref}} \quad (3.23)$$

The specific heat for the unknown material can be given by substituting equation 3.23 in 3.21

$$c_p = \left(\frac{C_{p_{ref}} m_{ref}}{\left(\frac{dt}{dT} \right) \left(\frac{dQ}{dt} \right)_{ref}} \right) \left[\left(\frac{1}{m} \right) \left(\frac{dt}{dT} \right) \left(\frac{dQ}{dt} \right) \right] \quad (3.24)$$

Reducing like terms in equation 3.24, the specific heat of the unknown material can be written as:

$$c_p = (C_{p_{ref}}) \left(\frac{m_{ref}}{m} \right) \left[\frac{\left(\frac{dQ}{dt} \right)}{\left(\frac{dQ}{dt} \right)_{ref}} \right] \quad (3.25)$$

3.3 Thermal Conductivity

Thermal conductivity is a fundamental property of solid materials as it described their ability to conduct heat. Understanding and controlling the thermal conductivity plays an important part in the design of power-dissipating devices and systems (Srivastava, 2006). When the density and specific heat of a material are known or can be determined, it is a consolidated

practice to experimentally evaluate the thermal diffusivity by transient methods and to calculate indirectly the thermal conductivity by the following equation (Cernuschi et al., 2004):

$$k = \rho c_p \alpha \quad (3.26)$$

The density values were provided by the developer of the materials. The thermal diffusivity and specific heat values were obtained by employing the methods described previously.

CHAPTER 4

Experimental Technique

4.1 The Flash Method – Thermal Diffusivity Measurement

4.1.1 Experimental Apparatus. In general, the ASTM E-1461 test standard delineates the minimum requirements for the apparatus used to determine thermal diffusivity. The key components are the flash source, specimen holder, temperature response detector, recording device, and an environmental enclosure when testing above and below room temperature (ASTM Standard E-1461, 2007) The flash source can be any device able to emit a quick energy pulse, usually a lamp or laser.



Figure 4.1. Flash Line™ 2000 Thermal Properties Analyzer and Data Acquisition System.

The apparatus used in this research was purchased from the Anter Corporation and is commercialized. The thermal property analyzer is the Flashline™ 2000 and is shown in Figure 4.1. It utilizes a High Speed Xenon Discharge lamp with safety interlocks as the pulse source (Anter). The pulse duration time should be less than 2% of the halftime of the specimen to be measured in order to keep the error due to finite pulse less than 0.5%. The apparatus is automated and capable of testing up to four specimens in each run, and its automatic sequencing of multiple

tests ensures high statistical reliability for the data obtained (Anter). Overall this indexed system has increased repeatability when compared with configurations that only allow one specimen to be tested at a time. The thermal property analyzer also contains a vacuum-capable environmental enclosure, in which nitrogen gas is used to evacuate the chamber. The detector should be any sensor that can measure a linear electrical output proportional to a small temperature rise. It along with its amplifier must have a response time of no more than 2% of the half-time. The temperature response InSb infrared detector outputs a linear electrical signal proportional to a small temperature change experienced by the rear face of the specimen after the pulse. The data acquisition system can be pre-programmed within one time period for the acceptable resolution of at least 1% for the quickest thermogram the system can deliver (ASTM Standard E-1461, 2007).

The Flashline™ 2000 apparatus adheres to all of the described requirements given by the ASTM testing standard E-1461, the standard test method for thermal diffusivity measurement by the flash method, as guaranteed by the manufacturer (Anter). Additionally, as provided by the manufacturer specifications, the following statements can be made. Thermal diffusivity measurements can be conducted from room temperature to 330°C. The flexibility of the apparatus allows for this range to be extended by the addition of supplemental furnaces or cooling chambers. The thermal diffusivity measurement range is 0.001 to 10 cm²/s with a repeatability of 2% and an accuracy of 4% . The Flashline™ 2000 also has the capability of measuring the specific heat of materials and directly calculating thermal conductivity when provided the density data. This feature was not used in this research. The initial cost of the device is approximately \$30,000 and there is little cost associated with each test run performed.

4.1.2 Test Specimen Preparation. The test specimens were prepared to be thin circular disks of 10 to 30 mm in diameter, whose front face surfaces are less than that of the energy pulse beam (ASTM 2007). According to ASTM E-1461 each specimen should be thick enough to be representative of the test material but remain close to the 1 to 6 mm range. Overall, the optimum thickness depends upon the magnitude of the estimated thermal diffusivity and should be chosen so that the time to reach half of the maximum temperature falls within the 10 to 1000 ms range. In order to accomplish these specified dimensions, a drill press equipped with a diamond plated drill bit was used to cut the material to the appropriate diameter. When necessary, the specimens were milled to achieve the preferred thickness.

Both the rear and front faces were flat and parallel within 0.5% of their thickness to maintain pulse uniformity. The standard suggests that a thin, uniform layer of graphite be applied to both faces of the specimens. The coating may be applied by spraying, painting, sputtering, etc (ASTM Standard E-1461, 2007). This will improve the capability of the specimen to absorb the energy applied, especially in case of highly reflective materials. For transparent materials, a layer of gold, silver, or other opaque material must be deposited first, followed by the graphite coating (ASTM Standard E-1461, 2007).

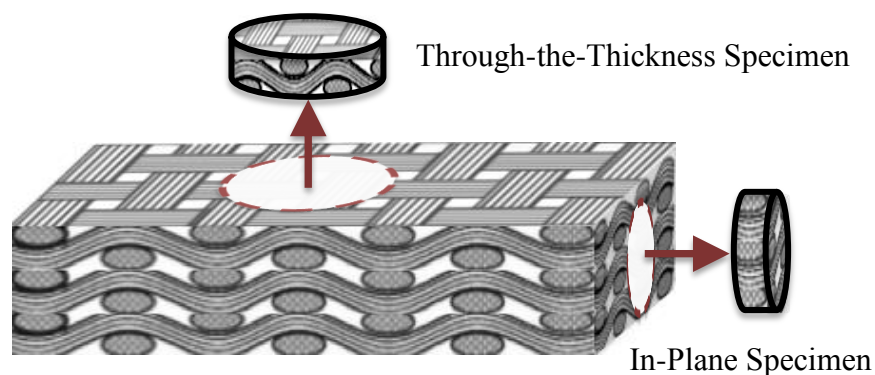


Figure 4.2. Schematic of Bulk Carbon-Carbon with Cylindrical Specimens.

None of the materials tested in this research are transparent; therefore no opaque coating was required. Applying the graphite coating was not necessary for all the experiments performed in this work due to the material nature of the plain weave 1K x 1K T300 carbon-carbon. However, the plain weave 3K x 3K T300 carbon-carbon samples were sprayed with a thin graphite coating due to their slightly reflective appearance. This preparation was executed for the in-plane (i-p) and through-the-thickness (t-t-t) test specimens as displayed in Figure 4.2. The average specifications of the flash method test specimens are given in Table 4.1.

Table 4.1

Average Specifications of Flash Method Test Specimens

Material	Diameter (mm)	Thickness (mm)	Mass (g)	Density (g/cm³)	Orientation	Fiber Tow
Carbon- Carbon	26.610	2.562	2.175	1.59	t-t-t	1K x 1K
Graphitized Carbon-Carbon	24.657	2.159	1.690	1.62	t-t-t	1K x 1K
Carbon-Carbon	12.510	1.737	0.335	1.63	t-t-t	3K x 3K
Carbon-Carbon	12.467	3.200	0.635	1.63	i-p	3K x 3K

4.1.3 Experimental Procedure. The experiments were conducted following the ASTM E-1461 test standard. 12.7 mm (0.5 inch) and 25.4 mm (1 inch) diameter samples prepared utilizing the definitions given previously. The diameter, thickness, mass, and density were measured and recorded. Using tweezers, each sample was placed in the specimen holder housed inside a sealed environmental enclosure. The environmental enclosure was purged using nitrogen gas to form an inert environment for the samples. A Dewar flask housed the liquid nitrogen to maintain its integrity. Approximately 1 L of liquid nitrogen was manually poured in the receptacle of the IR detector with the assistance of a funnel in order to prevent spilling. The

thickness, diameter, and mass parameters of each test specimen were input into the FlashLine™ 2000 System software, and the test temperature program was defined. For the experiments in this research the testing began at room temperature (25°C). Each sample was tested to a maximum temperature of 315°C. At each designated temperature, three flashes were performed at a time. The data acquisition system recorded the measurement from the three flashes and the average of these was used to define the value at each temperature. The results were compiled, analyzed, and necessary correction factors were applied. An equipment validation was conducted in order to verify the results obtained by the FlashLine™ 2000 device. The thermal diffusivity of the standard material, thermographite, was measured and the values were compared to published literature data.

4.2 Differential Scanning Calorimetry (DSC) – Specific Heat Measurement

4.2.1 Experimental Apparatus. The ASTM E-1269 test standard defines the testing conditions and essential apparatus capabilities for the specific heat measurement. The configuration must have a DSC test chamber equipped with a furnace, temperature sensor, differential sensor, and test chamber environmental enclosure. Additionally, there must be a temperature controller, signal recording device, crucibles, and a cooling capability (ASTM Standard E-1269, 2005). The calorimeter used to conduct the specific heat measurement in this research is a commercial apparatus, and it uses a technique in which the difference in the heat flow to a sample and to a reference is monitored as a function of time or temperature, while the sample and reference are subjected to a controlled temperature program (NETZSCH, 2008).

The DSC 200 F3 Maia®, Differential Scanning Calorimeter is manufactured by NETZSCH and is a heat flux system that combines high stability, high resolution, and fast response time throughout an extensive temperature range (NETZSCH, 2008). The apparatus is

equipped with a furnace block, sample chamber, cooling system, heat flux sensor, and a purge gas capability. Figure 4.3 depicts a cross-section schematic of the DSC 200 F3 Maia® measuring cell (NETZSCH, 2008) and Figure 4.4 displays the device. The furnace block contains a miniature, jacketed heater that provides uniform and controlled heating to the contents of the sample chamber. The heating rate can be defined between 0.001 K/min to 100 K/min. The furnace temperature is measured by a thermocouple integrated into the furnace wall (NETZSCH, 2008). The sample chamber is sealed within the instrument's lid, and has two additional lids to prevent impurities from the outside environment contaminating the test. The Intracooler 40 serves as the cooling system, and it allows for the apparatus to cool quickly from elevated temperatures and to achieve and sustain subambient temperatures (ASTM Standard E-1269, 2005). The Intracooler 40 also can attain cooling rates of 0.001 K/min to 70 K/min, and it extends the testing temperature range of the DSC 200 F3 Maia® from room temperature to cryogenic values yielding a spectrum of -40°C to 600°C .

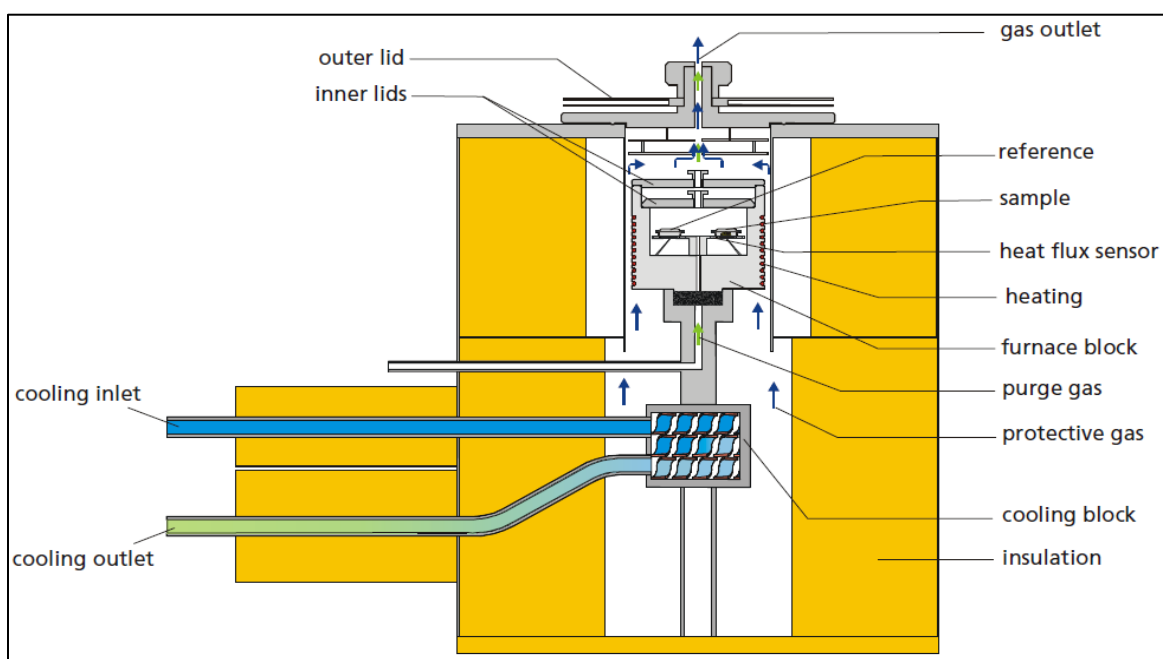


Figure 4.3. Cross-Section Schematic of the DSC.

The calorimeter utilizes a high sensitivity heat flux sensor and robust thermocouple wires as its differential and temperature indicators, respectively (NETZSCH, 2008). The purge gas capability of the apparatus can sustain the test chamber environment in an inert static or dynamic purge gas flow at rates of 10 to 50 mL/min. The device has a temperature controller that can execute specific temperature programs containing isothermal heating and cooling with a temperature accuracy of ± 0.1 K and an enthalpy accuracy of less than 1% (NETZSCH 2008). The digital recording device and the Proteus® Software allow the data acquisition system to record and display the heat flow signal as a function of time and temperature and can perform automatic baseline corrections (NETZSCH, 2008). Additionally, the measurement range is 0 to ± 600 mW.



Figure 4.4. Differential Scanning Calorimeter – DSC 200 F3 Maia®.

4.2.2 Test Specimen Preparation. When conducting the specific heat measurement using DSC, an adequate thermal contact between the heat flux sensor and the test specimen is essential for optimum results. In order to attain this condition, the specimen should be oriented such that it lays as even as possible with the bottom of the aluminum crucible. A 4-mm or 6-mm diameter and 1-mm thick sample can be used with this equipment using the corresponding crucible size. A cutting tool was used to achieve these sample dimensions. If necessary the flat

face of the sample was filed to the desired 1 mm thickness. Because the mass of the specimen is very important, all samples were carefully weighed three times on a balance of accuracy $\pm 0.00001\text{g}$ and the average mass was recorded. Table 4.2 describes the typical dimensions and mass for the DSC test specimens used in this research.

Table 4.2

Typical Dimensions of DSC Test Specimens

Material	Mass (mg)	Diameter (mm)
Carbon-Carbon (1K x 1K)	48.29	6
Graphitized Carbon-Carbon (1K x 1K)	44.69	6
Carbon-Carbon (3K x 3K)	25.86	4

Utilizing tweezers each sample was positioned into the center of the crucible pan, and the lid was situated on top of the crucible pan to ensure the sample was completely encased. An empty crucible pan and lid were also prepared in order to serve as the reference. Figure 4.5 displays a specimen centered inside the aluminum crucible pan with the accompanying lid.



Figure 4.5. DSC Test Specimen Inside Open Aluminum Crucible with Lid.

4.2.3 Experimental Procedure. The differential scanning calorimetry experiments were conducted following the guidelines in the ASTM E-1269, standard test method for determining specific heat. The DSC 200 F3 Maia® Measuring Cell and data acquisition device were turned on and allowed to initialize, while the Proteus® Software was opened. The argon gas was then turned on to allow the system to be purged. To attain an inert testing environment within the measuring cell the gas rate was set to 40 mL/min. A review of the device configurations via the software allows for the user to verify that the temperature calibration for the apparatus is up to date. In order to execute the specific heat measurement three tests are performed.

The first of the three tests is considered the baseline experiment. Because aluminum crucibles are used to house the test samples during the tests, there is an additional contact resistance present. The baseline run is deemed a correction for this contact resistance and increases the accuracy of the results. A baseline must be executed for the desired temperature program for each material. The software is set to correction and the temperature program is defined. Using tweezers, lids are affixed on two empty crucible pans. The empty crucibles are then carefully placed on the reference and sample locations of the heat flux sensor making sure the crucibles are centered on the sensors as shown in Figure 4.6 (Saad et al., 2011). The program begins at 20°C and is then cooled at a rate of 2 K/min to 5°C. At 5°C the samples are held isothermally at this temperature for 5 minutes. The cell is then heated to 320°C at a rate of 15 K/min and held isothermally for 5 minutes. To conclude the program the measurement cell is cooled to 40°C and held in standby mode and then to a final ambient temperature to protect the integrity of the apparatus. The apparatus transmits the heat signal to the data acquisition system and a thermal curve results. The thermal curve is representative of the thermal resistance versus temperature or time.

After the apparatus has reached ambient conditions the standard test can begin. Without removing the crucible from the heat flux sensor, the lid is removed and a sapphire reference material is placed inside. The crucible lid is returned and the software resets the apparatus. For this test run the parameters are set for correction and sample.

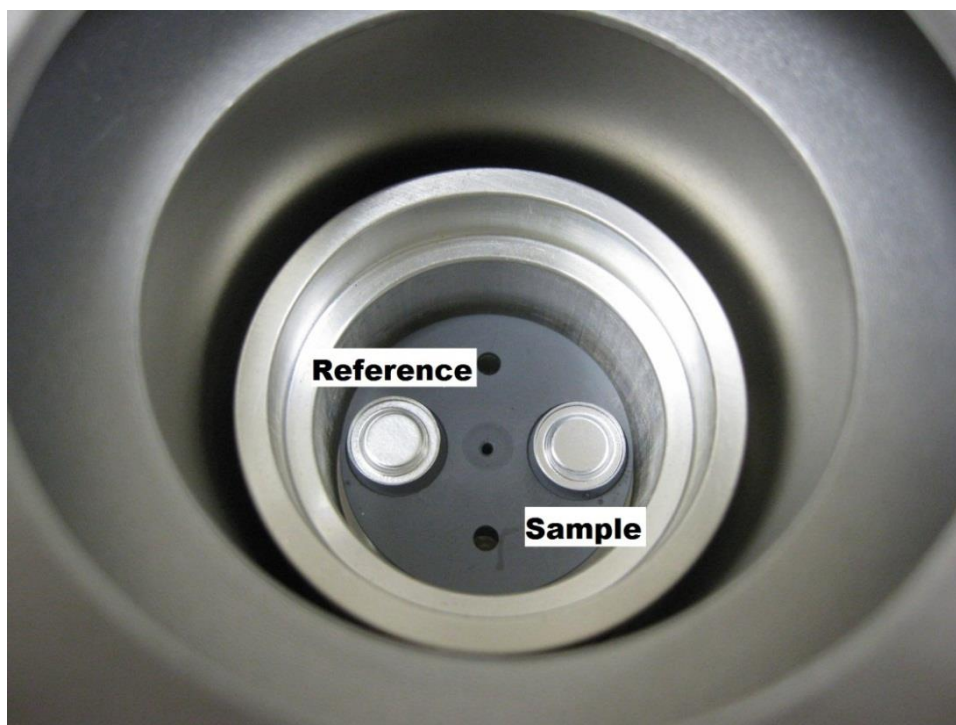


Figure 4.6. Crucibles Centered on the Heat Flux Sensors.

Now, the baseline correction will automatically be implemented into the data for the standard test run in order to correct the contact resistance added by the crucible. The identical temperature program is executed, this time for the empty crucible and the sapphire reference. Following this test, the sapphire is removed and replaced with the test specimen and the same temperature program is run for the third time. The device transmits the DSC signal to the data acquisition system where it is recorded. The heating segments of the sapphire and test specimen experiments are compared to the documented information for the sapphire reference, which is pre-programmed into the software. The ratio method is then used to determine the specific heat

of the material. This procedure was repeated for each sample material. In order to validate the measurements made by the DSC 200 F3 Maia® Measuring Cell device, temperature calibrations were performed every four months and the carbon-carbon specific heat results were compared to published data in literature for poco-graphite. The poco-graphite is used as comparison because its specific heat characteristics are similar to those of the carbon-carbon.

CHAPTER 5

Results

5.1 Thermal Diffusivity

The flash method was used to determine the in-plane and the through-the-thickness thermal diffusivity of the carbon-carbon composites. Three types of through-the-thickness samples were investigated, non-graphitized carbon-carbon (1K x 1K), graphitized carbon-carbon (1K x 1K), and non-graphitized carbon-carbon (3K x 3K). In addition, in-plane specimens of the non-graphitized carbon-carbon (3K x 3K) were analyzed.

An equipment validation was conducted in order to verify the results obtained by the FlashLine™ 2000 device. The thermal diffusivity of the standard material, thermographite, was measured and the values were compared to data published in literature. The measurements made by the device were deemed valid because the error varied only from approximately 0.105% to 5.35%. The comparison of the published and experimental data of the thermographite is shown in Figure 5.1. The published literature data was obtained from the International Journal of Thermophysics (Maglić & Milošević, 2004).

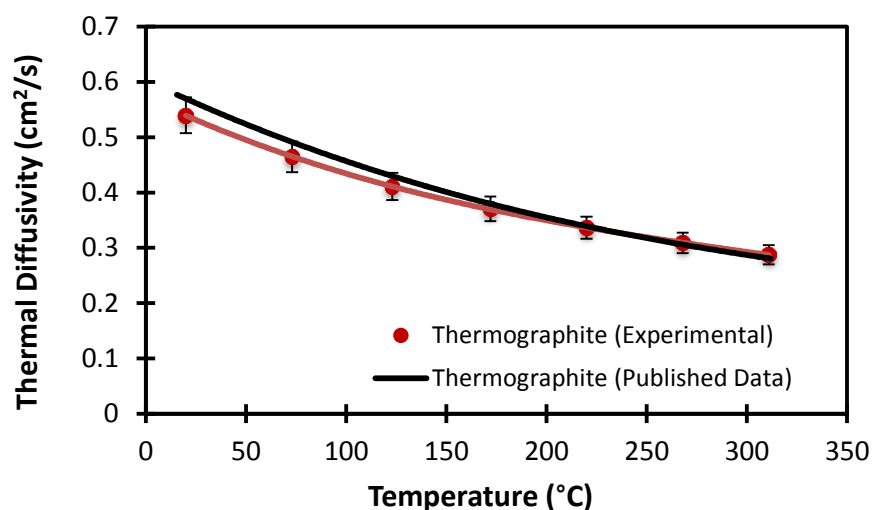


Figure 5.1. Published and Experimental Thermal Diffusivity Data of Thermographite.

The thermal diffusivity of the carbon-carbon composites was measured between room temperature and 330°C. This range was selected due to the temperature limitations of the apparatus. Figure 5.2 displays a magnified view of the error bars of the thermal diffusivity values of the carbon-carbon composite. In general, temperature has a minimal effect on the thermal diffusivity of carbon-carbon, where the values drop approximately 10% over the temperature range.

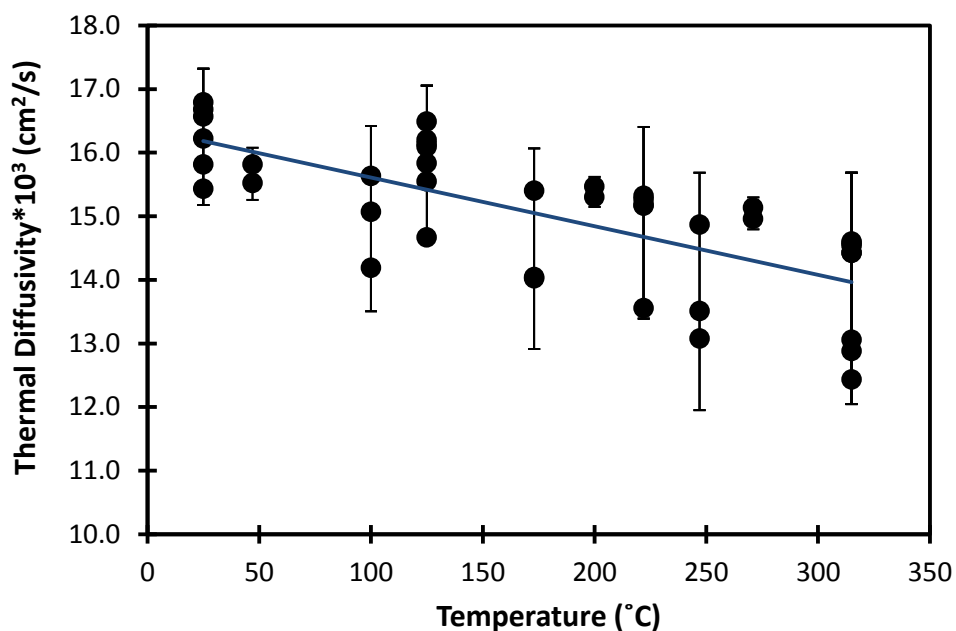


Figure 5.2. Through-The-Thickness Thermal Diffusivity of Carbon-Carbon (1K).

In contrast, the thermal diffusivity of the graphitized carbon-carbon dropped nearly 50% from room temperature to 315°C as shown in Figure 5.3. The thermal diffusivity of the graphitized carbon-carbon was more influenced by the temperature because of the large difference in the coefficient of thermal expansion between the matrix resin and fiber. At higher temperatures this expansion difference between the thermal behavior of the resin and fiber becomes more apparent, resulting in a sharp decrease in thermal diffusivity (Iqbal et al., 2011).

Heat-treating the graphitized material has already caused a permanent change on the matrix and fiber. This effect is increased when the material undergoes testing above room temperature.

A comparison of the graphitized and non-graphitized 1K x 1K carbon-carbon trend lines in Figure 5.3 further shows that the diffusivity values of the graphitized carbon-carbon are 8.9 times those of the non-graphitized composites. The large difference between the thermal diffusivity values is due to the effect of graphitization on the composite.

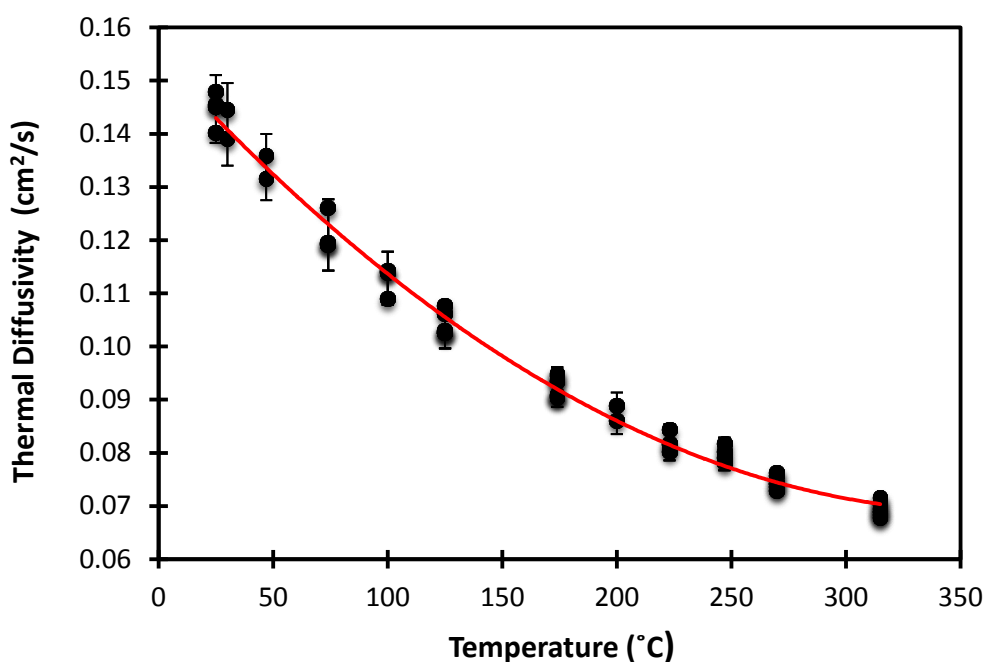


Figure 5.3. Through-The-Thickness Thermal Diffusivity of Graphitized Carbon-Carbon (1K).

Graphitization is the transformation of a standard carbon structure into a higher ordered graphite structure. The order increase can be observed as a shift from an amorphous carbon structure to a sequence of stacked parallel plates. The graphitization process takes place at temperatures greater than 2500°C. The structural shift begins slowly near 1800°C and then occurs at a more rapid rate as temperature increases. Hydrogen, sulfur, and other impurities abscond from the material between 1200°C and 2000°C. Eventually, the carbon crystals grow from 5 nm to 100 nm or larger. Additionally, the spacing between the carbon layers begins to

decrease and density increases. It is observed that a decreased structural order will tend to significantly reduce the thermal conductivity of a material (Saad et al., 2011). Because the structural order of the graphitized samples is increased this causes them to have a significantly higher thermal diffusivity than the non-graphitized composites as apparent in Figure 5.4. The maximum thermal diffusivity occurs at room temperature. The measured experimental values of thermal diffusivity in this research are similar to those found for comparable materials in investigations reported in a NASA Technical Memorandum (Ohlhorst et al., 1997)

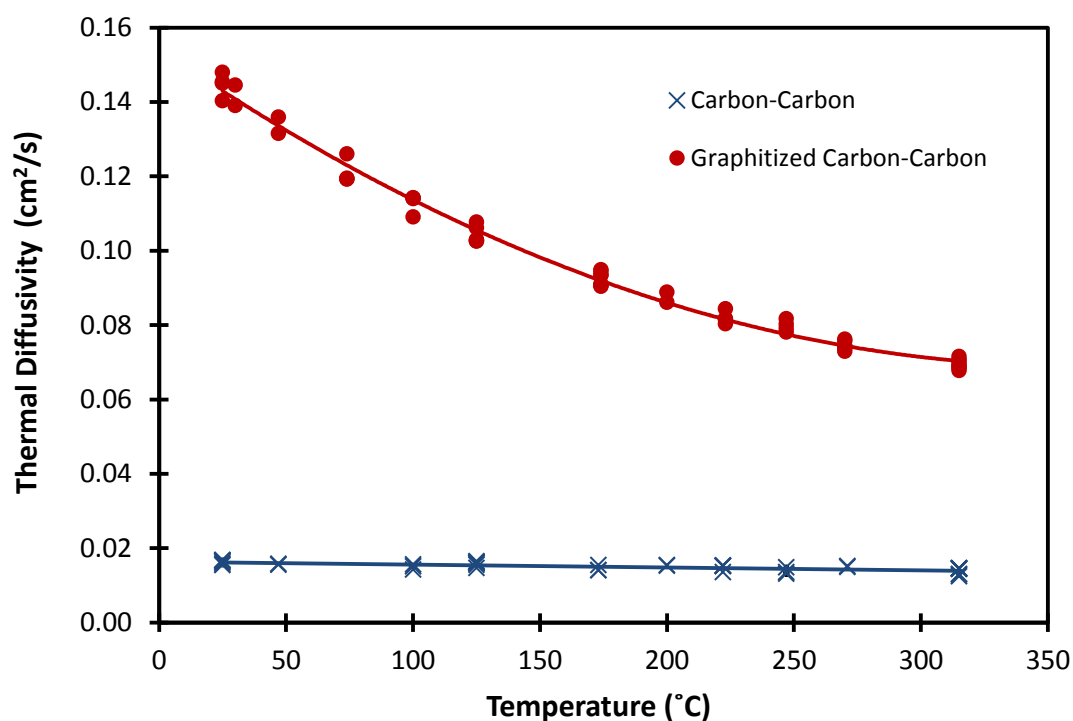


Figure 5.4. Comparison of Through-The-Thickness Thermal Diffusivity of Carbon-Carbon.

The non-graphitized 3K x 3K carbon-carbon material was tested in order to compare the in-plane and through-the-thickness thermal diffusivity values. These samples also allowed for the evaluation of the effect of coating samples with graphite. The thermal diffusivity measurements of these samples were also conducted from room temperature to 330°C. Figure 5.5 exhibits the through-the-thickness thermal diffusivity values of the 3K x 3K carbon-carbon composite.

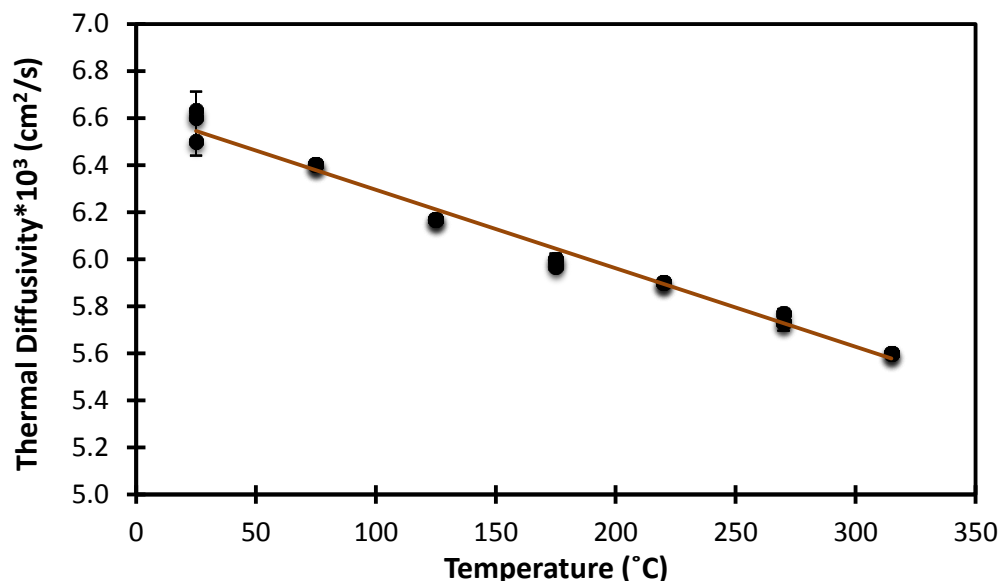


Figure 5.5. Through-The-Thickness Thermal Diffusivity of Carbon-Carbon (3K).

The diffusivity decreases as temperature increases, and the trend in the data is nearly linear. In a comparison of the room temperature measurement to the highest temperature tested, the diffusivity quantity reduced approximately 15%. As shown in Figure 5.6, the in-plane thermal diffusivity of the 3K x 3K carbon-carbon also has a linear trend and there was nearly an 11% decrease from room temperature to 315°C. Coinciding with the results of the diffusivity measurements of the 1K x 1K non-graphitized carbon-carbon, the thermal diffusivity is not greatly influenced by an increase in temperature. Consistent with the findings in the NASA Technical Memorandum, for both in-plane and through-the-thickness directions, thermal diffusivity values are maximum at room temperature and decrease with increasing temperature (Ohlhorst et al., 1997)

A comparison of the in-plane and through-the-thickness thermal diffusivity measurements of the 3K x 3K non-graphitized carbon-carbon is displayed in Figure 5.7. Here it can be found that the in-plane values are approximately 3.7 times higher than that of the through-the-thickness quantities.

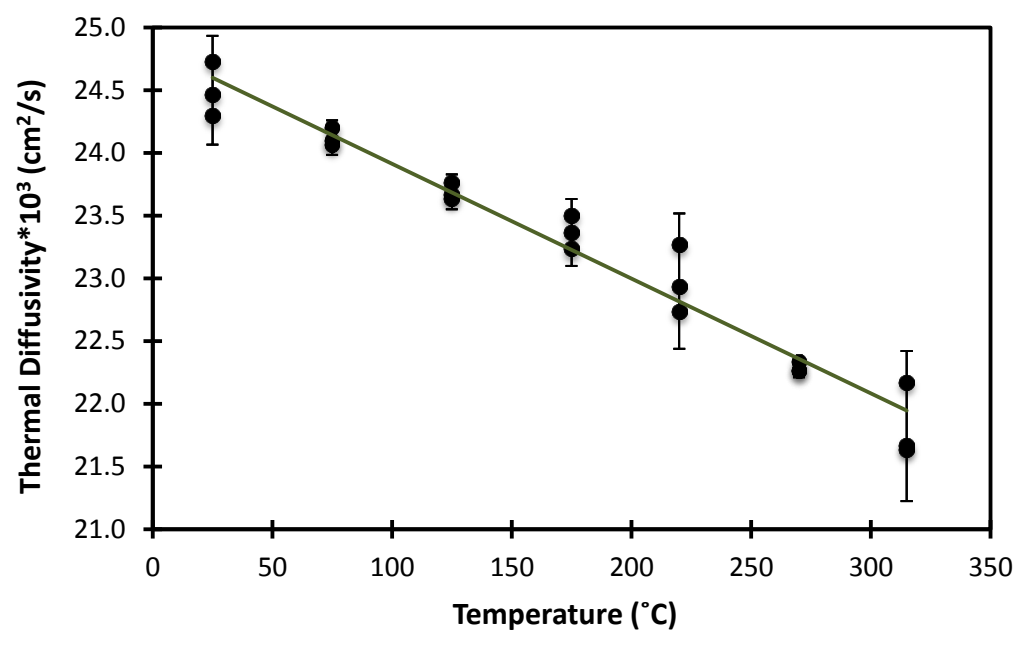


Figure 5.6. In-Plane Thermal Diffusivity of Carbon-Carbon (3K).

During the in-plane propagation of heat through the material, the heat can travel quickly along the fiber. For the through-the-thickness case, the heat must travel across the fiber and through the resin where the resin has a much lower thermal diffusivity resulting in a lower thermal diffusivity of the composite.

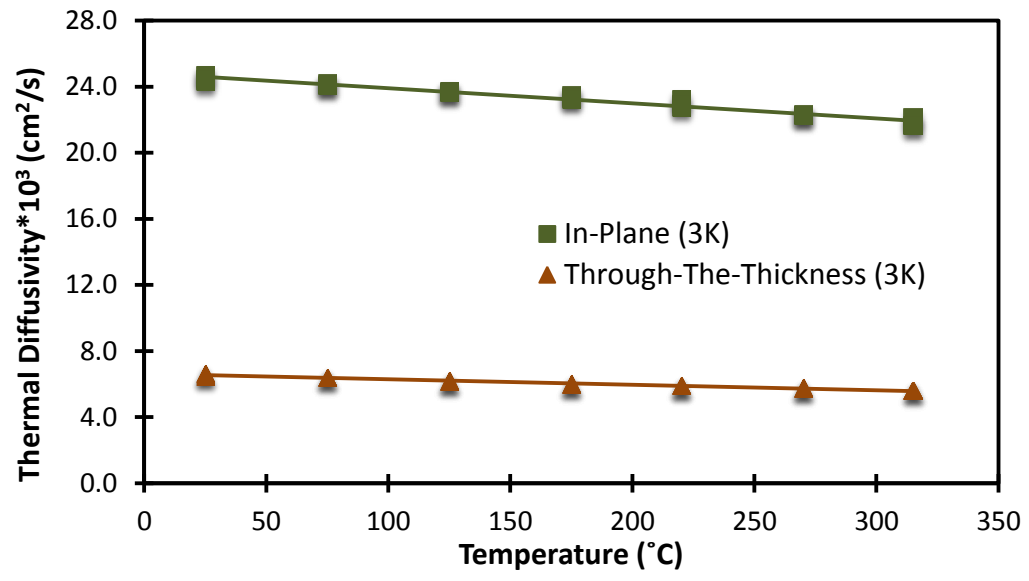


Figure 5.7. In-Plane and Through-The-Thickness Thermal Diffusivity of Carbon-Carbon (3K).

An additional and final thermal diffusivity experiment was conducted in order to analyze the effect the graphite coating has on the measurement. Figure 5.8 displays the coated and not coated in-plane thermal diffusivity of 3K x 3K carbon-carbon trend lines. The trend lines overlap at some points and the greatest percent difference existing between the lines is only 1.75%. The trend lines based on the coated and not coated through-the-thickness thermal diffusivity of the 3K x 3K carbon-carbon are shown in Figure 5.9. The lines neither intersect nor overlap and the percent difference is nearly 23.2%. From a comparison of these coated and not coated results it can be concluded that the graphite coating has a minimal effect on the in-plane measurements while it has a greater influence on the through-the-thickness values.

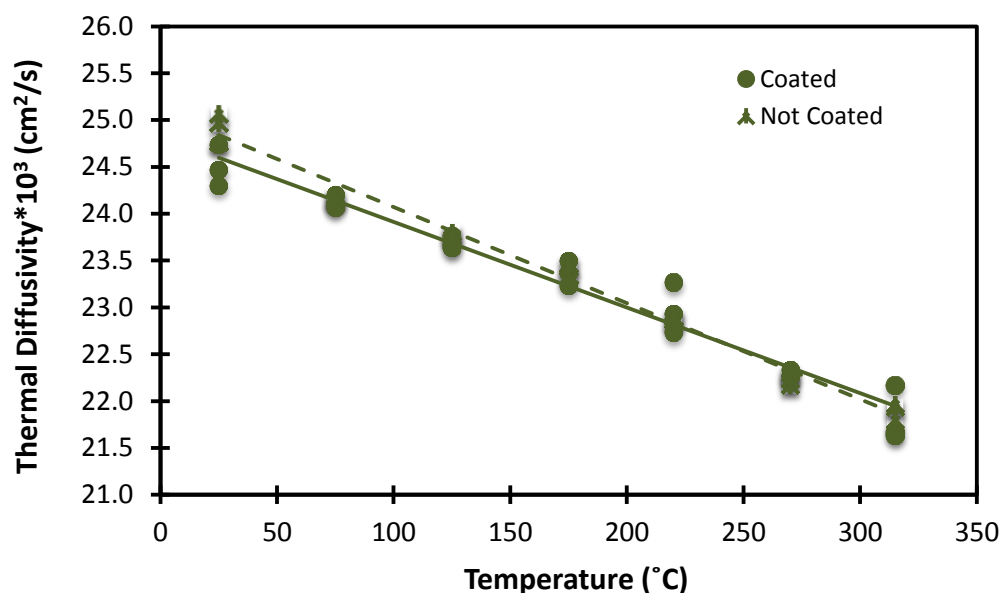


Figure 5.8. Effect of Coating on In-Plane Thermal Diffusivity of Carbon-Carbon.

According to the ASTM E-1461 test standard, the graphite coating improves the capability of the specimen to absorb the energy flash. Thermal diffusivity of the specimen describes how quickly it can conduct heat through its thickness. Since the in-plane values are significantly higher than the through-the-thickness values, this means the in-plane samples are better conductors.

A better conductor will show less improvement when coated as compared to a material with a lower thermal diffusivity. Overall, there is smaller percent difference between the in-plane coated and not coated specimens than between the t-t-t coated and not coated specimens because i-p samples have a greater thermal diffusivity and are better conductors of heat.

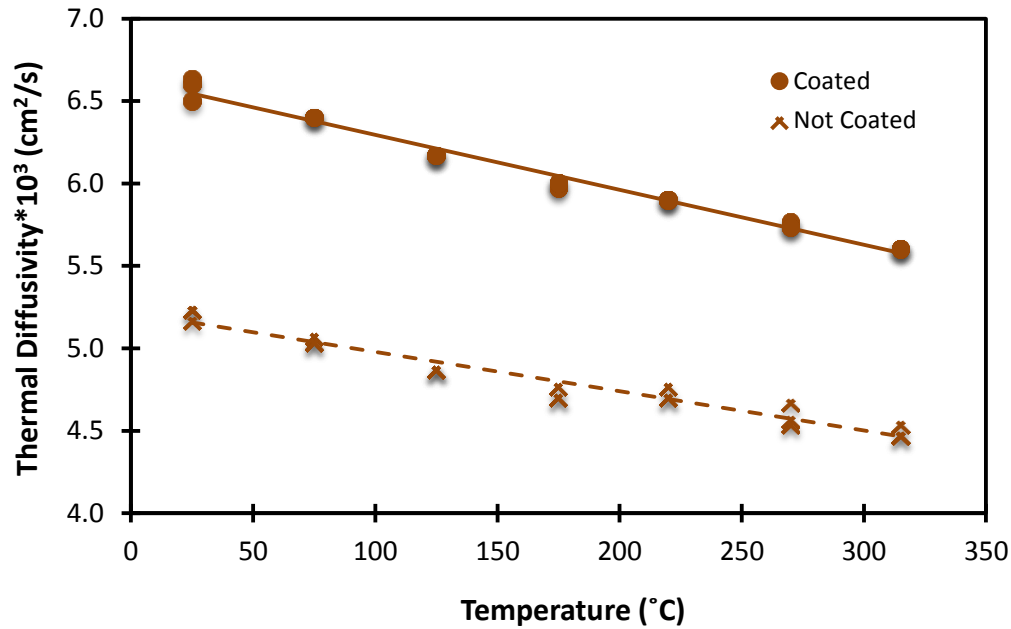


Figure 5.9. Coating Effect on Through-The-Thickness Thermal Diffusivity of Carbon-Carbon.

Experimental results provide the statistical estimates known as the population mean value and the population standard deviation defined by (Figliola & Beasley, 2011)

$$\sigma = \sqrt{\frac{1}{N} \sum_{i=1}^N (a_i - \bar{a})^2} \quad (5.1)$$

The results from each temperature tested are considered as a population, where N is the total number of measurements, a_i represents a single i^{th} measurement, and \bar{a} is the mean value of the data at each temperature. Additionally, the margins of errors were calculated for each temperature using standard deviation of the mean as shown in equation 5.2.

$$SE = \frac{\sigma}{\sqrt{N}} \quad (5.2)$$

The critical value from the normal distribution chart based on 95% confidence is 1.96, and the margin of error or confidence interval, e , is determined by the following

$$e = \pm 1.96 \cdot SE \quad (5.3)$$

After these values have been determined for a set of data, it can be stated that there is a 95% confidence that the true mean value of the data will lie within the mean quantity plus or minus the margin of error. For example, when the room temperature thermal diffusivity measurement is conducted on a through-the-thickness 1K x 1K carbon-carbon composite, 95% percent of the time the measured value will be with the range of 0.016250 ± 0.000121 cm²/s. Additionally, the percent error can now be found using equation 5.4.

$$error \% = \left(\frac{e}{mean} \right) \times 100 \% \quad (5.4)$$

The error was calculated at each temperature, and the error bars shown in Figures 5.2, 5.3, 5.5 and 5.6 indicate a two standard deviation range about the associated data. This range depicts the interval of values in which 95% of the thermal diffusivity measurements should lie. Summaries of the error results at selected temperatures for each type of thermal diffusivity specimen are given in Tables 5.1, 5.2, 5.3, and 5.4.

Table 5.1

Thermal Diffusivity Results for Carbon-Carbon (1K-ttt)

Temperature (°C)	Mean (cm ² /s)	Standard Deviation (cm ² /s)	Margin of Error (cm ² /s)	Percent Error (%)
25	0.016250	0.000513	± 0.000121	1.459
125	0.015851	0.000558	± 0.000239	1.505
315	0.013865	0.000860	± 0.000344	2.480

An analysis of the results given in Tables 5.1 and 5.2 will reveal that the percent error associated with the 1K x 1K fiber tow graphitized carbon-carbon composites is less than the error experienced by the non-graphitized 1K x 1K fiber tow carbon-carbon composites. This occurs because the graphitized carbon-carbon is much more conductive than the non-graphitized carbon-carbon, allowing heat to travel much faster with less losses and therefore less error.

Table 5.2

Thermal Diffusivity Results for Graphitized Carbon-Carbon (1K-ttt)

Temperature (°C)	Mean (cm ² /s)	Standard Deviation (cm ² /s)	Margin of Error (cm ² /s)	Percent Error (%)
25	0.144686	0.002865	± 0.001621	1.120
125	0.104120	0.002036	± 0.000941	0.903
315	0.069505	0.001182	± 0.000473	0.681

The increased diffusivity of the graphitized composites allows the energy pulse to propagate through the material much faster resulting in less radiation heat loss from the sample and therefore less error. Similarly, comparing the in-plane and through-the-thickness 3Kx 3K fiber tow carbon-carbon composites, the in-plane samples experience less error because of their higher thermal diffusivity as shown in Tables 5.3 and 5.4.

Table 5.3

Thermal Diffusivity Results for Carbon-Carbon (3K-ttt)

Temperature (°C)	Mean (cm ² /s)	Standard Deviation (cm ² /s)	Margin of Error (cm ² /s)	Percent Error (%)
25	0.006578	0.000057	±0.000064	0.975
125	0.006179	0.000021	±0.000021	0.340
270	0.005744	0.000009	±0.000018	0.310

Table 5.4

Thermal Diffusivity Results for Carbon-Carbon (3K-ip)

Temperature (°C)	Mean (cm ² /s)	Standard Deviation (cm ² /s)	Margin of Error (cm ² /s)	Percent Error (%)
25	0.024500	0.000178	± 0.000202	0.824
125	0.023689	0.000057	± 0.000064	0.271
270	0.022289	0.000031	± 0.000036	0.160

According to the ASTM E-1461 (2005) testing standard, the optimum thickness of the test specimen should be selected such that the time to reach half of the maximum temperature (half-time), $t_{1/2}$ falls within the 10 to 1000 ms (0.01 to 1 s) range. To verify that the samples were fabricated to the proper thickness, an initial test was performed to analyze the half-times of the test samples. The half-times reached at each temperature during this experiment were recorded and can be found in Figure 5.10. The documented half-times for each material at the specified temperature were within the acceptable range as defined by the testing standard and are shown in Figure 5.10 with dashed lines. This signifies that appropriate thicknesses were chosen for the test samples. It can be observed that the half-times of the graphitized carbon-carbon composite are nearly an order of magnitude lower than those of the carbon-carbon composite. The graphitized carbon-carbon composites have shorter half-times because they are more conductive which allows the energy pulse to propagate through the material much faster than in the non-graphitized carbon-carbon. Similarly, for the 3K x 3K carbon-carbon composites, the in-plane half-times were shorter than the through-the-thickness half-times because heat travels much quicker along the fiber resulting in less radiation heat losses.

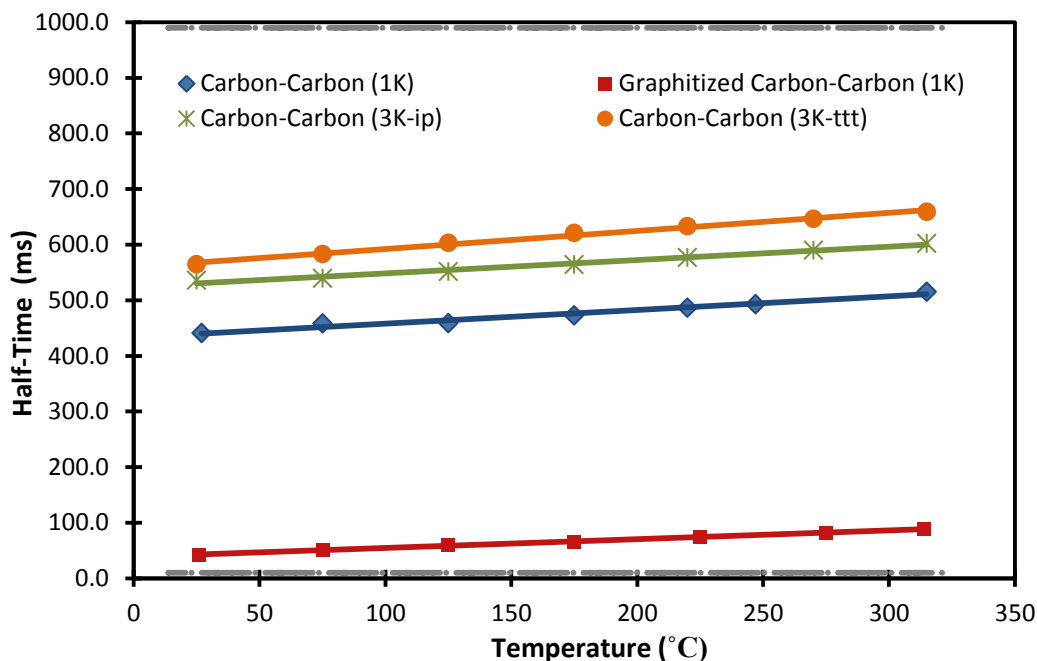


Figure 5.10. Half-Times of Tested Materials Compared to Allowable Limits.

The temperature and time data can also be analyzed using thermogram curves. Normalized thermograms can be developed by incorporating the half-time and maximum temperature values into the data. The normalized thermogram curves can be compared to the theoretical model in order to depict and explain shape differences. Figure 5.11 shows the thermogram temperature curves for the 1K x 1K carbon-carbon composite and the theoretical model. As the ratio of time to halftime increases and the ratio of temperature change to maximum temperature approaches unity, it can be observed that the experimental temperature curves differ more and more from the theoretical model. Figure 5.12 displays a comparison of the normalized theoretical thermogram to a thermogram of experimental data that experienced radiation heat losses (ASTM Standard E-1461, 2007). Using this figure from the ASTM E-1461 testing standard it can be concluded that the deviations in Figure 5.11 are due to radiation heat losses. It can be observed that at lower temperatures (i.e. cryogenic), there are significant losses in comparison to those losses experienced as higher temperatures.

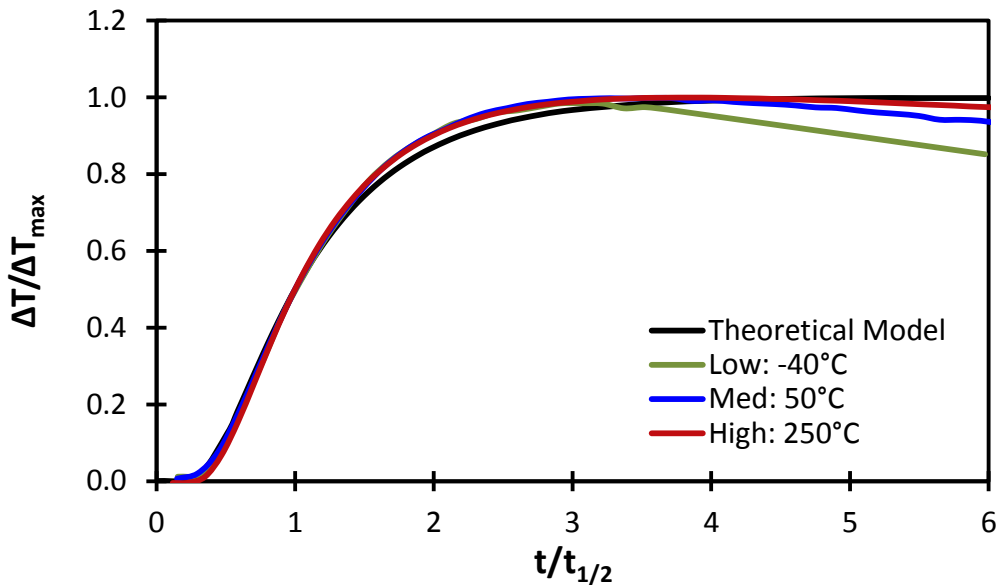


Figure 5.11. Comparison of the Carbon-Carbon Thermograms to the Theoretical Model.

Overall there is an inverse correlation, the higher the test temperature the lower the amount of radiation heat loss ($T^4(t) - T_\infty^4$) where $T(t)$ corresponds to the temperature of the sample after the instantaneous energy pulse. Figure 5.11 shows the thermograms for $T_\infty = -40^\circ\text{C}$, 50°C , 250°C . T_∞ represents the initial temperature of the sample as well as the ambient temperature immediately before the flash occurs.

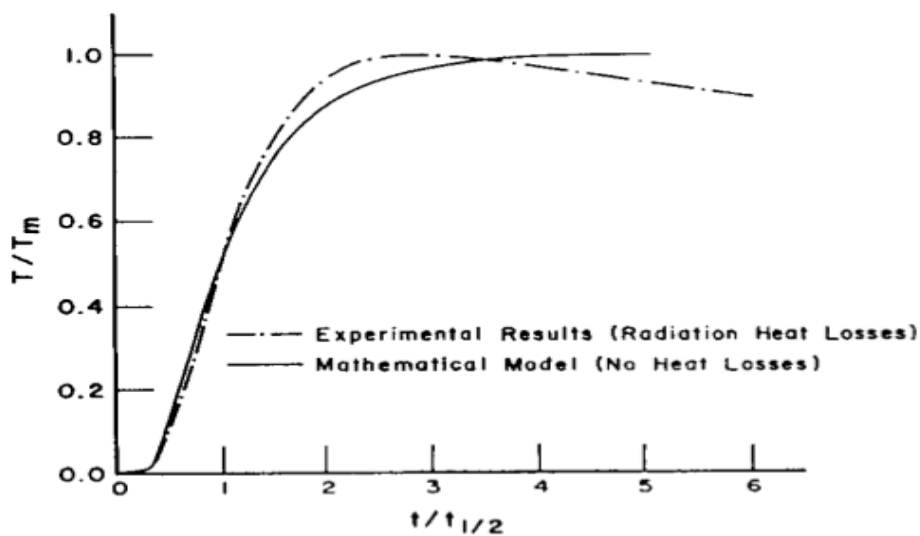


Figure 5.12. Rear Face Temperature Rise: Mathematical Model versus Experimental Result.

Therefore at a higher temperature testing environment the radiation heat loss is less than the radiation heat loss at a lower test environment temperature (Patrick & Saad, 2012). Analysis of these results also led to the selection of an appropriate correction factor. The Clark and Taylor correction factor contains adjustments for radiation heat losses and is therefore suitable for the materials in this research.

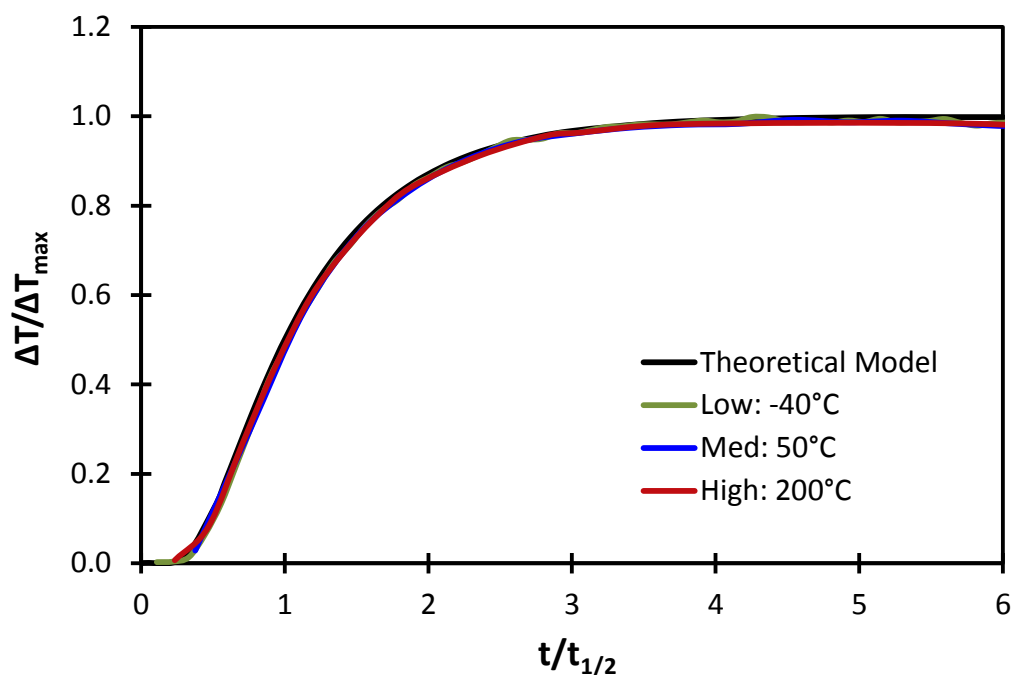


Figure 5.13. Graphitized Carbon-Carbon Thermograms Versus the Theoretical Model.

The 1K x 1K graphitized carbon-carbon thermograms are shown in Figure 5.13 and, the radiation heat loss is minimal for all of the temperatures tested. The graphitized test specimens experienced less radiation heat loss because the energy pulse travels very quickly through the material allowing less radiation losses from the material. This rapid travel of heat through the graphitized samples is verified by Figure 5.10, depicting low half-times for these specimens at all temperatures. Similar results were also found for the 3K x 3K carbon-carbon composite material as shown in Figure 5.14. As temperature increased radiation heat losses decreased.

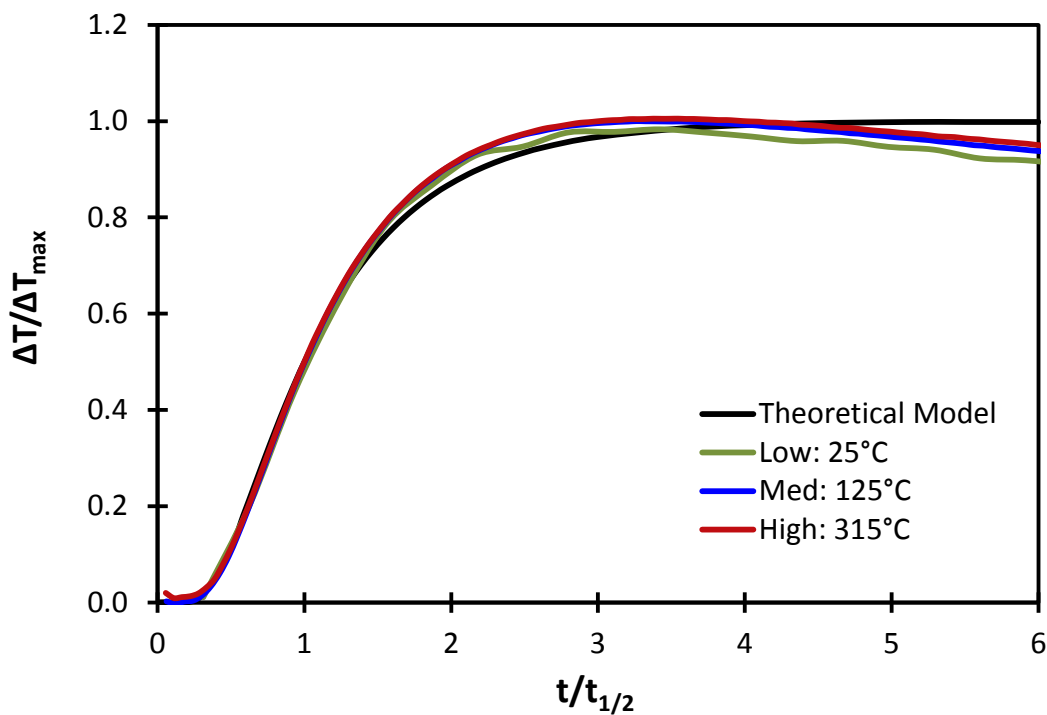


Figure 5.14. Carbon-Carbon (3K) Thermograms Versus the Theoretical Model.

5.2 Specific Heat

Differential scanning calorimetry was utilized to measure the specific heat of the carbon-carbon composites. Three types were investigated, non-graphitized carbon-carbon (1K x 1K), graphitized carbon-carbon (1K x 1K), and non-graphitized carbon-carbon (3K x 3K). In order to validate the measurements made by the DSC 200 F3 Maia® Measuring Cell device, temperature calibrations were performed every four months and were checked with data for the standard indium material. Additionally, the carbon-carbon specific heat results were compared with a reference material. In this research poco-graphite was used as the reference material, and the published data was obtained from Poco-Graphite, Incorporated (Poco-Graphite, 2001). The values measured by the DSC device were deemed valid because the poco-graphite and carbon-carbon have good agreement as shown in Figure 5.15.

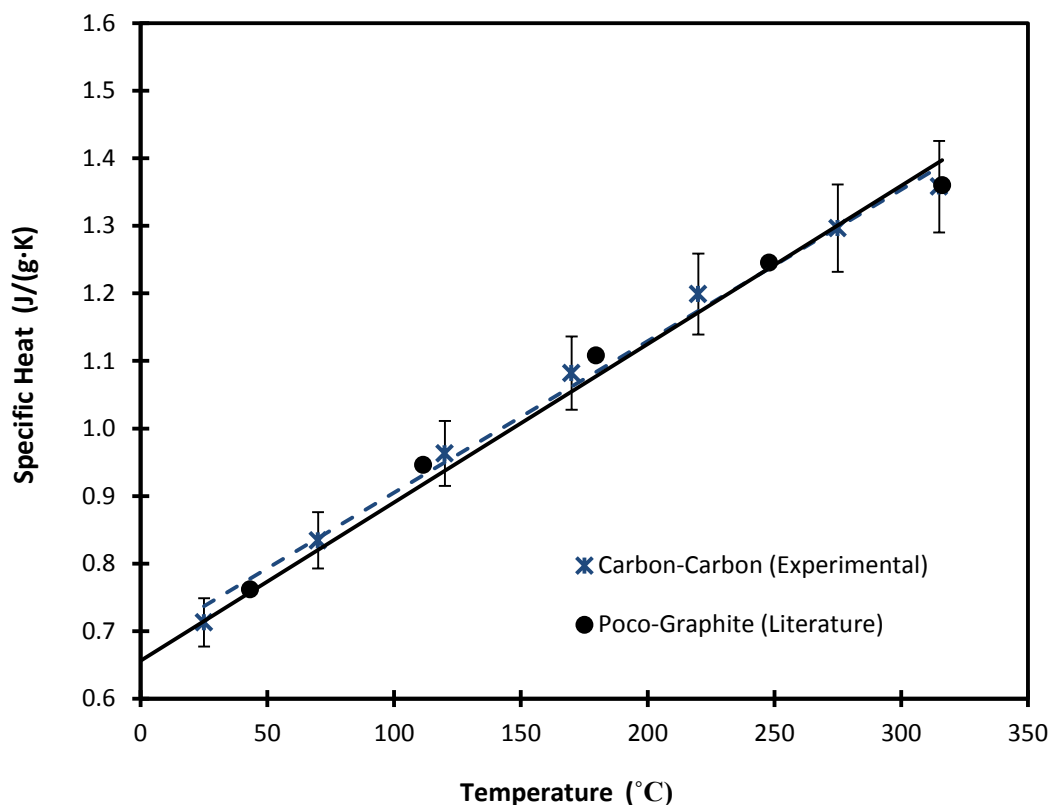


Figure 5.15. Specific Heat of Carbon-Carbon Versus Poco-Graphite.

The specific heat measurements of the carbon-carbon (1K x 1K), the graphitized carbon-carbon (1K x 1K), carbon-carbon (3K x 3K) composites all show trends that are extremely close to linear. A comparison of the results can be found in Figure 5.16. For all three types of samples tested there is a direct correlation. As the testing temperature increases, the specific heat of the material increases. The specific heat of graphitized carbon-carbon is approximately 2.5 % higher than that of the non-graphitized carbon-carbon. Additionally, the specific heat trend line of the carbon-carbon (3K x 3K) composite is not parallel to the trend lines of the other materials because of the difference in the carbon fabric. The decreased slope of the carbon-carbon (3K x 3K) composite specific heat curve occurs because its specific heat is less dependent upon temperature change than the carbon-carbon (1K x 1K) composites.

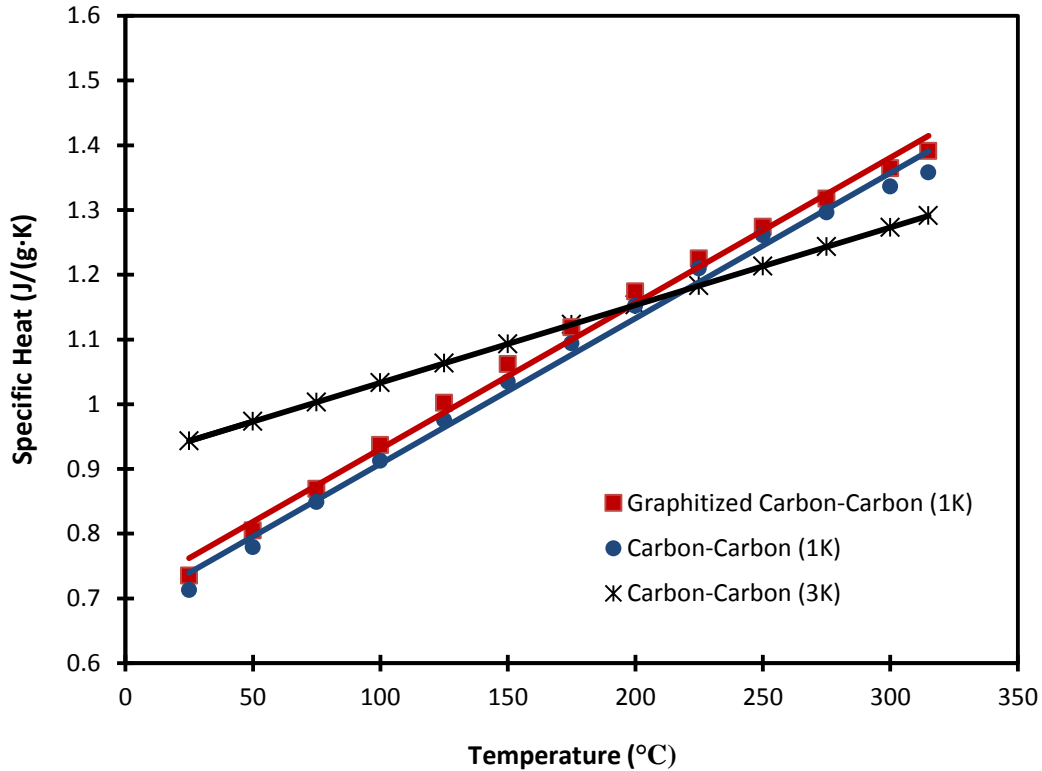


Figure 5.16. Specific Heat of Tested Materials.

5.3 Thermal Conductivity

Utilizing the density, specific heat, and thermal diffusivity data, the thermal conductivity values of the composite materials were calculated using the following equation:

$$k = \rho c_p \alpha \quad (5.5)$$

The resulting thermal conductivity values of the 1K x 1K carbon-carbon and graphitized carbon-carbon composites are compared in Figure 5.17. The thermal conductivity of the graphitized carbon-carbon composite is an order of magnitude higher than that of the non-graphitized. The increase in thermal conductivity is due to the increase in the crystallinity of the graphitized material when compared to the non-graphitized material (Iqbal et al., 2011). Additionally, impurities such as hydrogen and sulfur are no longer present in the material. The removal of

impure substances from the material and the shift of the carbon layers to a more closely packed arrangement further contribute to the increase in the thermal conductivity. The thermal conductivity results obtained in this investigation are similar to those found for analogous materials in the investigation conducted by Ohlhorst *et al.* (1997).

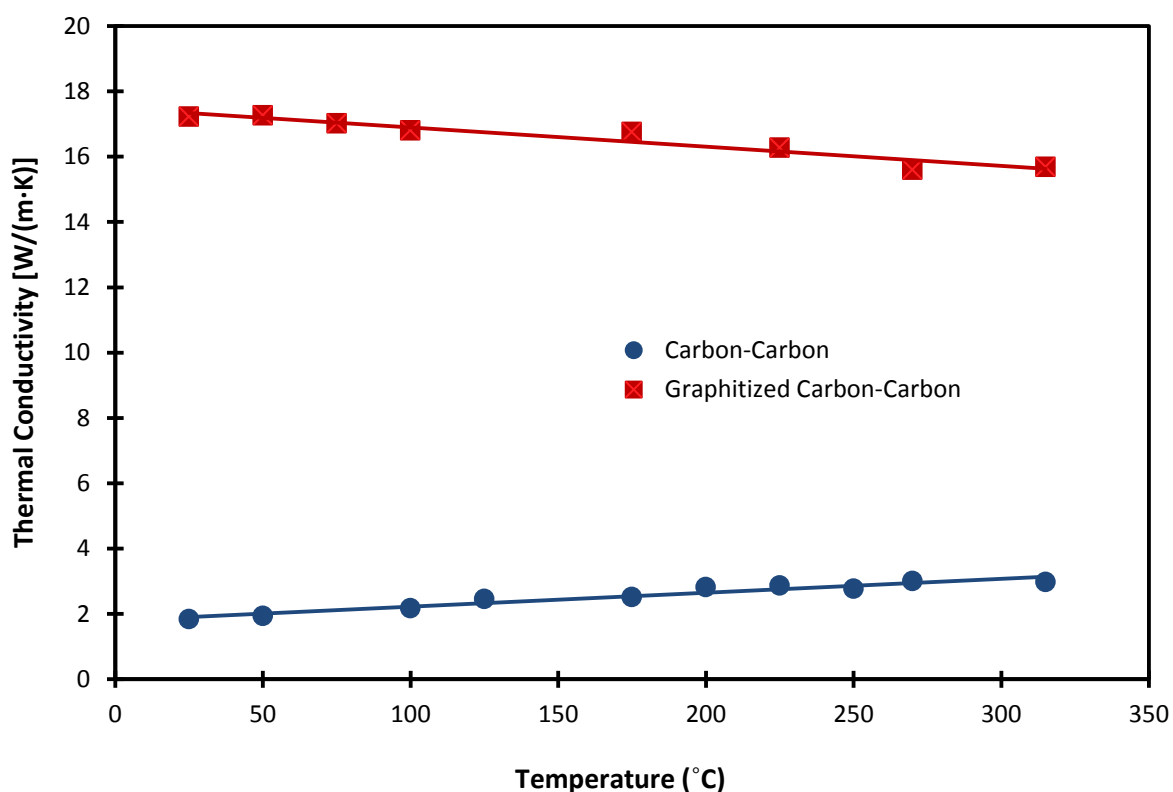


Figure 5.17. Thermal Conductivity Comparison of Carbon-Carbon (1K).

The thermal conductivity results of the in-plane and through-the-thickness 3K x 3K carbon-carbon are displayed in Figure 5.18. The in-plane thermal conductivity is higher than the through-the-thickness conductivity because the heat is able to transfer longitudinally along the fiber much better than across the fiber. Additionally, in the through-the-thickness direction the heat must also transfer across the resin, which has a much lower thermal conductivity; this results in a lower overall thermal conductivity of the composite.

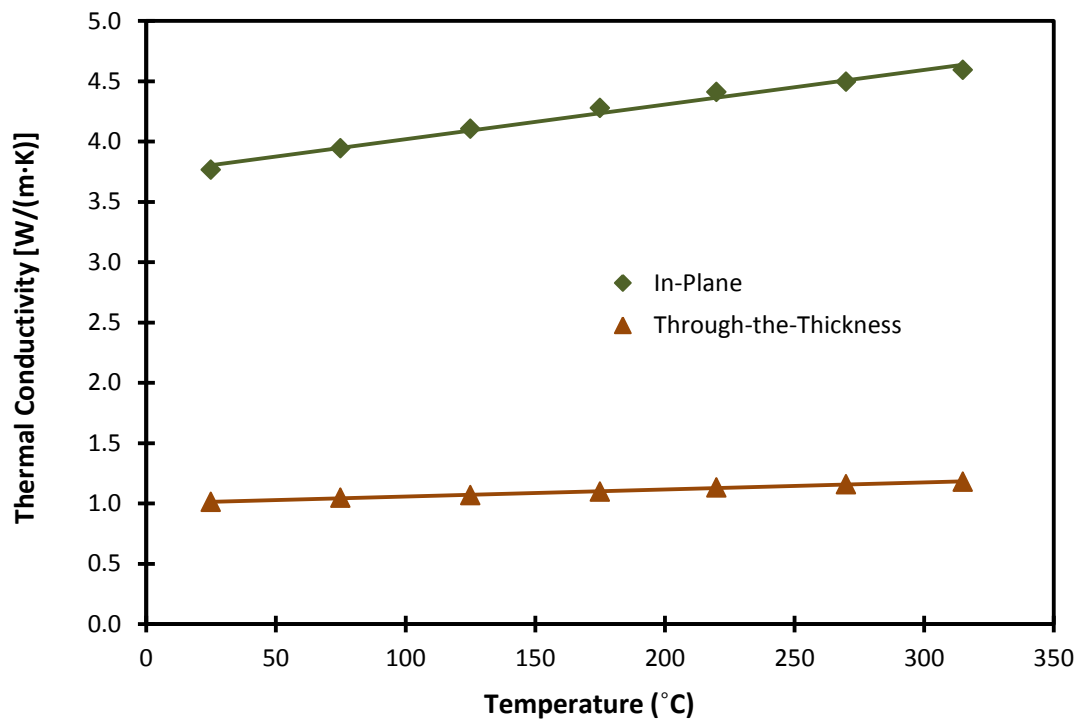


Figure 5.18. Thermal Conductivity of In-Plane and Through-The-Thickness Carbon-Carbon.

The thermal property results found in this research were compared to those obtained using the laser flash device at Oak Ridge National Laboratory and the findings were in good agreement. Additionally, Table 5.5 gives a summary of the thermal property results at room temperature (25°C) for all the materials tested in this research.

Table 5.5

Thermal Property Results at Room Temperature

Material	Density (g/cm ³)	Specific Heat (J/g·K)	Thermal Diffusivity (cm ² /s)	Thermal Conductivity (W/m·K)	Orientation
Carbon- Carbon (1K)	1.59	0.7130	0.0163	1.84	t-t-t
Graphitized Carbon-Carbon (1K)	1.62	0.7354	0.1447	17.2	t-t-t
Carbon-Carbon (3K)	1.63	0.9433	0.0066	1.01	t-t-t
Carbon-Carbon (3K)	1.63	0.9433	0.0245	3.77	i-p

CHAPTER 6

Discussion and Future Research

6.1 Discussion

An examination of the through-the-thickness and in-plane thermal properties of carbon-carbon composites from room temperature to 330°C was conducted in this research. The thermal diffusivity was measured using the flash method. Analyses were performed to validate the accuracy of the thermal diffusivity results. The DSC was used to measure the specific heat of the materials. The specific heat of the composites was determined using the heating curves of the differential scanning calorimeter. The thermal conductivity was determined using the density, specific heat, and thermal diffusivity of the composites. The graphitized material exhibited different thermal properties than the non-graphitized material due to the effect of the heat treatment. Due to the increased crystallinity of the graphitized material during the heat treatment the thermal conductivity of the graphitized material is greater than that of the non-graphitized. The in-plane thermal conductivity of the 3K x 3K carbon-carbon is higher than the through-the-thickness conductivity because heat transfers more readily along the fibers than it does across the fibers and through the resin.

6.2 Future Research

There are several recommendations for future research.

- The in-plane thermal diffusivity measurements on the graphitized carbon-carbon should be conducted.
- Develop an equation to calculate the through-the-thickness thermal conductivity of a composite using the volume fraction and conductivity values of the

constituents when the conductivity of the fiber and resin are not similar. These theoretical values could then be compared to the experimental results.

- The thermal properties database should continue to be developed by adding data for other composite materials and foams.
- Examine the effect that the other correction factors have on the thermal diffusivity measurements.

References

- Adams, P. M., Katzman, H. A., Rellick, G. S., & Stupian, G. W. (1998). Characterization of High Thermal Conductivity Carbon Fibers and a Self-Reinforced Graphite Panel. *Carbon*, 36(3), 233-245. doi: [http://dx.doi.org/10.1016/S0008-6223\(97\)00189-9](http://dx.doi.org/10.1016/S0008-6223(97)00189-9)
- Anter. FlashLine™ Thermal Diffusivity Measuring System Operation and Maintenance Manual Part 1 Flashline 2000.
- ASTM Standard E-1269. (2005). Standard Test Method for Determining Specific Heat Capacity by Differential Scanning Calorimetry. West Conshohocken, PA: ASTM International.
- ASTM Standard E-1461. (2007). Standard Test Method for Thermal Diffusivity by the Flash Method. West Conshohocken, PA: ASTM International.
- Beck, J. V., & Dinwiddie, R. B. (1995). Parameter Estimation Method for Flash Thermal Diffusivity with Two Different Heat Transfer Coefficients. *23rd International Thermal Conductivity Conference*, 123-136.
- Cernuschi, F., Bison, P. G., Figari, A., Marinetti, S., & Grinzato, E. (2004). Thermal Diffusivity Measurements by Photothermal and Thermographic Techniques. *International Journal of Thermophysics*, 25(2), 439-457.
- Cernuschi, F., Bison, P. G., Marinetti, S., Figari, A., Lorenzoni, L., & Grinzato, E. (2002). Comparison of Thermal Diffusivity Measurement Techniques. *Quantitative InfraRed Thermography Journal*, 28.
- Chawla, K. (1998). *Composite Materials: Science and Engineering* (2nd ed.). New York: Springer Science+Business Media, Inc.
- Chen, Y. J., Ren, X. J., Zhang, P., Zhang, T., & Wu, A. B. (2012). Measurement of Thermal Conductivity of CFRPs and Thermal Conductance of the Cold-to-Warm Joint at Low

- Temperatures. *IEEE Transactions on Applied Superconductivity*, 22(3), 7700704-7700704. doi: <http://dx.doi.org/10.1109/tasc.2011.2177231>
- Clark, L. M., & Taylor, R. E. (1975). Radiation Loss in the Flash Method for Thermal Diffusivity. *Journal of Applied Physics*, 46(2), 714-719.
doi: <http://dx.doi.org/10.1063/1.321635>
- Czichos, H., Saito, T., & Smith, L. (2006). *Springer Handbook of Materials Measurement Methods*. Germany: Springer Science+Business Media, Inc.
- Daniel, I. M., & Ishai, O. (2006). *Engineering Mechanics of Composite Materials* (2nd ed.). New York: Oxford University Press.
- Figliola, R. S., & Beasley, D. E. (2011). *Theory and Design for Mechanical Measurements* (5th ed.): John Wiley & Sons.
- Grujicic, M., Zhao, C. L., Dusel, E. C., Morgan, D. R., Miller, R. S., & Beasley, D. E. (2006). Computational Analysis of the Thermal Conductivity of the Carbon–Carbon Composite Materials. *Journal of Materials Science*, 41(24), 8244-8256. doi: <http://dx.doi.org/10.1007/s10853-006-1003-x>
- Hahn, D. W., & Özışik, M. N. (2012). *Heat Conduction* (3rd ed.). New Jersey: John Wiley & Sons, Inc.
- Hashin, Z. (1983). Analysis of Composite Materials - A Survey. *Journal of Applied Mechanics*, 50(3), 481-505. doi: <http://dx.doi.org/10.1115/1.3167081>
- Höhne, G., Hemminger, W. F., & Flammersheim, H. J. (2003). *Differential Scanning Calorimetry*. Germany: Springer - Verlag Berlin Heidelberg.
- Hull, D., & Clyne, T. W. (1996). *An Introduction to Composite Materials*. New York: Cambridge University Press.

- Iqbal, S. S., Dinwiddie, R., Porter, W., Lance, M., & Filip, P. (2011). Effect of Heat Treatment on Thermal Properties of Pitch-Based Carbon Fiber and Pan-Based Carbon Fiber Carbon-Carbon Composites. *Mechanical Properties and Performance of Engineering Ceramics and Composites VI*, 32, 245-254. doi: <http://dx.doi.org/10.1002/9781118095355.ch23>
- Klett, J., & Conway, B. *Thermal Management Solutions Utilizing High Thermal Conductivity Graphite Foams*. Oak Ridge National Laboratory Retrieved from http://www.ornl.gov/~webworks/cpr/rpt/106741_.pdf.
- Luo, R., Liu, T., Li, J., Zhang, H., Chen, Z., & Tian, G. (2004). Thermophysical Properties of Carbon/Carbon Composites and Physical Mechanism of Thermal Expansion and Thermal Conductivity. *Carbon*, 42(14), 2887-2895. doi: <http://dx.doi.org/10.1016/j.carbon.2004.06.024>
- Maglić, K. D., & Milošević, N. D. (2004). Thermal Diffusivity Measurements of Thermographite. *International Journal of Thermophysics*, 25(1), 237-247.
- Manocha, L. (2003). High performance Carbon-Carbon Composites. *Sadhana*, 28(1-2), 349-358. doi: <http://dx.doi.org/10.1007/bf02717143>
- Mutnuri, B. (2006). *Thermal Conductivity Characterization of Composite Materials*. (M.S.M.E. 1436649), West Virginia University, United States -- West Virginia. Retrieved from <http://search.proquest.com/docview/304974295?accountid=12711> ProQuest Dissertations & Theses (PQDT) database.
- NETZSCH. (2008). Operating Instructions DSC 200 F3 Maia Selb, Germany.
- Nunes dos Santos, W. (2007). Thermal Properties of Polymers by Non-Steady-State Techniques. *Polymer Testing*, 26(4), 556-566. doi: <http://dx.doi.org/10.1016/j.polymertesting.2007.02.005>

- Ohlhorst, C. W., Vaughn, W. L., Ransone, P. O., & Tsou, H.-T. (1997). Thermal Conductivity Database of Various Structural Carbon-Carbon Composite Materials *NASA Technical Memorandum* (Vol. 4787, pp. 1-96): National Aeronautics and Space Administration, Langley Research Center.
- Parker, W. J., Jenkins, R. J., Butler, C. P., & Abbott, G. L. (1961). Flash Method of Determining Thermal Diffusivity, Heat Capacity, and Thermal Conductivity. *Journal of Applied Physics*, 32(9), 1679-1684. doi: <http://dx.doi.org/10.1063/1.1728417>
- Patrick, M., & Saad, M. (2012). Examination of Carbon-Carbon and Graphitized Carbon-Carbon Composites. *Frontiers in Heat and Mass Transfer*, 3(4). doi: <http://dx.doi/10.5098/hmt.v3.4.3007>
- Poco-Graphite. (2001). Properties and Characteristics of Graphite For Industrial Applications. In R. G. Sheppard, D. M. Mathes & D. J. Bray (Eds.). Decatur, TX.
- Saad, M., Baker, D., & Reaves, R. (2011). *Thermal Characterization of Carbon-Carbon Composites*. Paper presented at the ASME Conference Proceedings, Denver, Colorado, USA. doi: <http://dx.doi.org/10.5098/hmt.v3.4.3007>
- Srivastava, G. P. (2006). Lattice Thermal Conduction Mechanism in Solids. In S. L. Shinde & J. Goela (Eds.), *High Thermal Conductivity Materials* (1st ed.). New York: Springer-Verlag.
- Takezawa, Y. (2005). Novel High Thermal Conductive Epoxy Resins. *Electrical Insulation News in Asia Magazine*, 12, 43-44.
- Wei, J. (1989). Carbon Fiber Thermal Conductivity Measurement and Analysis (Defense Technology Information Center Technical Report Database, Trans.): Beijing Institute of Materials Science.

Wetherhold, R. C., & Wang, J. (1994). Difficulties in the Theories for Predicting Transverse Thermal Conductivity of Continuous Fiber Composites. *Journal of Composite Materials*, 28(15), 1491-1498. doi: <http://dx.doi.org/10.1177/002199839402801507>

Appendix

The following flash method mathematical analysis is provided in order to give a complete derivation of the thermal diffusivity.

Utilizing the equation for the temperature distribution within a thermally insulated solid of uniform thickness, L , developed by Carslaw and Jeager (1959), a mathematical expression to calculate thermal diffusivity was derived (Parker et al., 1961).

$$T(x, t) = \frac{1}{L} \int_0^L T(x, 0) dx + \frac{2}{L} \sum_{n=1}^{\infty} \exp\left(\frac{-n^2 \pi^2 \alpha t}{L^2}\right) \cos \frac{n\pi x}{L} \int_0^L T(x, 0) \cos \frac{n\pi x}{L} dx \quad (1)$$

where α is the thermal diffusivity in cm^2/s . If a pulse of radiant energy, Q (J/cm^2), is instantaneously and uniformly absorbed into a small depth referred to as g , at the front face ($x=0$) of the thermally insulated solid material (Clark & Taylor, 1975), the temperature distribution at the initial condition is given by:

$$T(x, 0) = \frac{Q}{\rho C_p g} \quad \text{for } 0 < x < g \quad (2)$$

$$T(x, 0) = 0 \quad \text{for } g < x < L \quad (3)$$

where ρ is the density and c_p is the specific heat capacity of the material. With the above initial conditions, equation 1 can be expressed as:

$$T(x, t) = \frac{1}{L} \left[\int_0^g \frac{Q}{\rho C_p g} dx + \int_g^L 0 \cdot dx \right] + \frac{2}{L} \sum_{n=1}^{\infty} \exp\left(\frac{-n^2 \pi^2}{L^2} \alpha t\right) \cos \frac{n\pi x}{L} \left[\int_0^g \frac{Q}{\rho C_p g} \cos \frac{n\pi x}{L} dx + \int_g^L 0 \cdot \cos \frac{n\pi x}{L} dx \right] \quad (4)$$

$$T(x, t) = \frac{1}{L} \left[\frac{Qx}{\rho C_p g} \right]_0^g + \frac{2}{L} \sum_{n=1}^{\infty} \exp\left(\frac{-n^2 \pi^2}{L^2} \alpha t\right) \cos \frac{n\pi x}{L} \left[\frac{QL}{\rho C_p g n \pi} \sin \frac{n\pi x}{L} \right]_0^g \quad (5)$$

$$T(x, t) = \frac{1}{L} \left[\frac{Qg}{\rho C_p g} - \frac{Q0}{\rho C_p g} \right] + \frac{2}{L} \sum_{n=1}^{\infty} \exp\left(\frac{-n^2 \pi^2}{L^2} at\right) \cos \frac{n\pi x}{L} \left(\frac{QL}{\rho C_p g n \pi}\right) \left[\sin \frac{n\pi g}{L} - \sin \frac{n\pi 0}{L} \right] \quad (6)$$

$$T(x, t) = \frac{1}{L} \left[\frac{Qg}{\rho C_p g} \right] + \frac{2}{L} \sum_{n=1}^{\infty} \exp\left(\frac{-n^2 \pi^2}{L^2} at\right) \cos \frac{n\pi x}{L} \left(\frac{QL}{\rho C_p g n \pi}\right) \left[\sin \frac{n\pi g}{L} \right] \quad (7)$$

$$T(x, t) = \frac{1}{L} \left[\frac{Q}{\rho C_p} \right] + \frac{2}{L} \sum_{n=1}^{\infty} \exp\left(\frac{-n^2 \pi^2}{L^2} at\right) \cos \frac{n\pi x}{L} \left(\frac{QL}{\rho C_p g n \pi}\right) \left[\sin \frac{n\pi g}{L} \right] \quad (8)$$

$$T(x, t) = \frac{Q}{\rho C_p L} \left[1 + 2 \sum_{n=1}^{\infty} \exp\left(\frac{-n^2 \pi^2 at}{L^2}\right) \cos \frac{n\pi x}{L} \cdot \left(\frac{L}{n\pi g}\right) \sin \frac{n\pi g}{L} \right] \quad (9)$$

$$T(x, t) = \frac{Q}{\rho C_p L} \left[1 + 2 \sum_{n=1}^{\infty} \exp\left(\frac{-n^2 \pi^2 at}{L^2}\right) \cos \frac{n\pi x}{L} \cdot \frac{\sin \frac{n\pi g}{L}}{\frac{n\pi g}{L}} \right] \quad (10)$$

For materials that are opaque to the energy pulse, the adsorption depth, g , is a very small number. It then it follows that

$$\sin \frac{n\pi g}{L} \cong \frac{n\pi g}{L} \quad (11)$$

$$\cos n\pi = (-1)^n \quad (12)$$

Once these are applied, the temperature distribution at the rear face ($x=L$) is expressed as (Parker et al., 1961):

$$T(L, t) = \frac{Q}{\rho C_p L} \left[1 + 2 \sum_{n=1}^{\infty} \exp\left(\frac{-n^2 \pi^2 at}{L^2}\right) \cos \frac{n\pi L}{L} \cdot \frac{\frac{n\pi g}{L}}{\frac{n\pi g}{L}} \right] \quad (13)$$

$$T(L, t) = \frac{Q}{\rho C_p L} \left[1 + 2 \sum_{n=1}^{\infty} \exp\left(\frac{-n^2 \pi^2 \alpha t}{L^2}\right) \cos n\pi \cdot 1 \right] \quad (14)$$

$$T(L, t) = \frac{Q}{\rho C_p L} \left[1 + 2 \sum_{n=1}^{\infty} (-1)^n \exp\left(\frac{-n^2 \pi^2 \alpha t}{L^2}\right) \right] \quad (15)$$

Setting

$$T_m = \frac{Q}{\rho C_p L} \quad (16)$$

where T_m is the maximum temperature at the rear face. (Parker et al., 1961) then defined two dimensionless parameters, V and ω as:

$$V(L, t) = \frac{T(L, t)}{T_m} \quad (17)$$

$$\omega = \frac{\pi^2 \alpha t}{L^2} \quad (18)$$

Substituting equation 18 into 15 yields:

$$T(L, t) = \frac{Q}{\rho C_p L} \left[1 + 2 \sum_{n=1}^{\infty} (-1)^n \exp(-n^2 \omega) \right] \quad (19)$$

$$\frac{T(L, t)}{\frac{Q}{\rho C_p L}} = \left[1 + 2 \sum_{n=1}^{\infty} (-1)^n \exp(-n^2 \omega) \right] \quad (20)$$

Now equation 17 can be substituted in for the left side of the equation

$$V(L, t) = \left[1 + 2 \sum_{n=1}^{\infty} (-1)^n \exp(-n^2 \omega) \right] \quad (21)$$

$$V = \left[1 + 2 \sum_{n=1}^{\infty} (-1)^n \exp(-n^2 \omega) \right] \quad (22)$$

Setting $V = 0.5$ allows for the determination of ω at the time required for the rear face to reach half of the maximum temperature rise.

$$0.5 = \left[1 + 2 \sum_{n=1}^{\infty} (-1)^n \exp(-n^2 \omega) \right] \quad (23)$$

$$-0.5 = 2 \sum_{n=1}^{\infty} (-1)^n \exp(-n^2 \omega) \quad (24)$$

$$-0.25 = \sum_{n=1}^{\infty} (-1)^n \exp(-n^2 \omega) \quad (25)$$

At $n=1$

$$-0.25 = (-1)^1 \exp(-1^2 \omega) \quad (26)$$

$$-0.25 = -\exp(-\omega) \quad (27)$$

$$0.25 = \exp(-\omega) \quad (28)$$

$$0.25 = e^{-\omega} \quad (29)$$

$$\ln(0.25) = \ln(e^{-\omega}) \quad (30)$$

$$1.38629 = \omega \quad (31)$$

At $n=2$

$$-0.25 = (-1)^1 \exp(-1^2 \omega) + (-1)^2 \exp(-2^2 \omega) \quad (32)$$

$$-0.25 = -\exp(-\omega) + \exp(-4\omega) \quad (33)$$

$$0.25 = e^{-\omega} - e^{-4\omega} \quad (34)$$

At n=3

$$-0.25 = (-1)^1 \exp(-1^2 \omega) + (-1)^2 \exp(-2^2 \omega) + (-1)^3 \exp(-3^2 \omega) \quad (35)$$

$$-0.25 = -\exp(-\omega) + \exp(-4\omega) + (-\exp(-9\omega)) \quad (36)$$

$$0.25 = e^{-\omega} - e^{-4\omega} + e^{-9\omega} \quad (37)$$

At n=4

$$-0.25 = (-1)^1 \exp(-1^2 \omega) + (-1)^2 \exp(-2^2 \omega) + (-1)^3 \exp(-3^2 \omega) + (-1)^4 \exp(-4^2 \omega) \quad (38)$$

$$-0.25 = -\exp(-\omega) + \exp(-4\omega) + (-\exp(-9\omega)) + \exp(-16\omega) \quad (39)$$

$$0.25 = e^{-\omega} - e^{-4\omega} + e^{-9\omega} - e^{-16\omega} \quad (40)$$

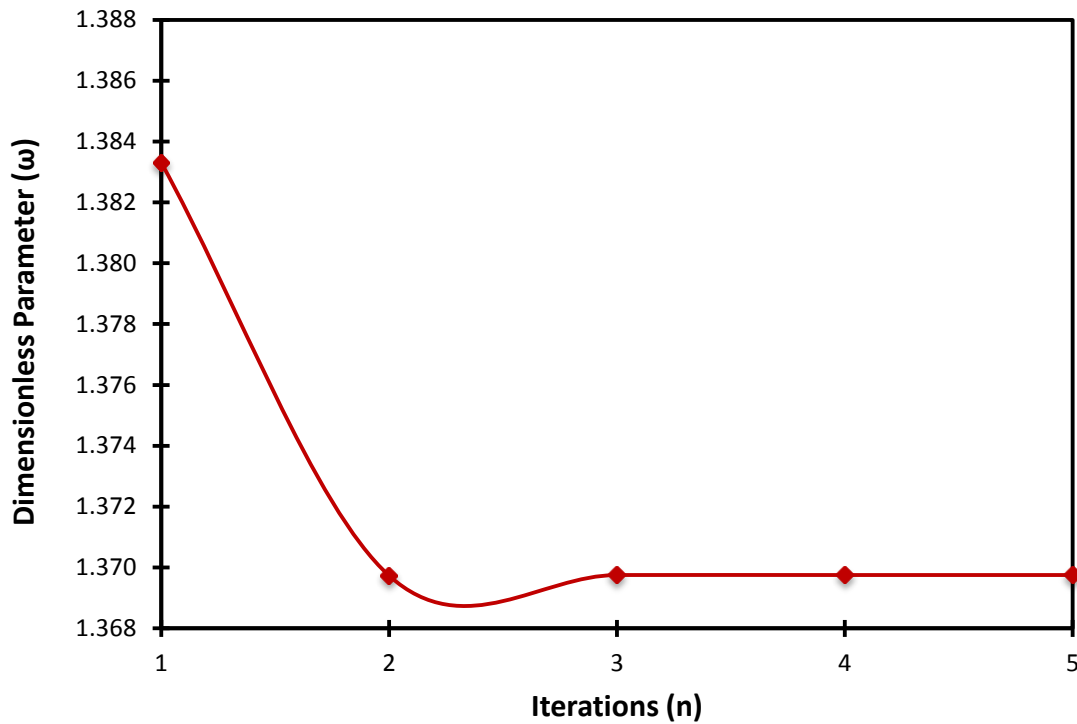
At n=5

$$\begin{aligned} -0.25 = & (-1)^1 \exp(-1^2 \omega) + (-1)^2 \exp(-2^2 \omega) + (-1)^3 \exp(-3^2 \omega) + (-1)^4 \exp(-4^2 \omega) \\ & + (-1)^5 \exp(-5^2 \omega) \end{aligned} \quad (41)$$

$$-0.25 = -\exp(-\omega) + \exp(-4\omega) + (-\exp(-9\omega)) + \exp(-16\omega) + (-\exp(-25\omega)) \quad (42)$$

$$0.25 = e^{-\omega} - e^{-4\omega} + e^{-9\omega} - e^{-16\omega} + e^{-25\omega} \quad (43)$$

Excel was used to calculate values of the right side of the equation at different ω values. The following figure shows that after three iterations ($n = 3$) the value of ω converges at 1.36975.



Substituting $\omega = 1.36975$ into equation 18 and making $t = t_{1/2}$ (since $V = 0.5$ was used) allows for a mathematical equation for thermal diffusivity to be stated as (Parker et al., 1961):

$$1.36975 = \frac{\pi^2 \alpha t}{L^2} \quad (44)$$

$$\alpha = \frac{1.36975 L^2}{\pi^2 t_{1/2}} \quad (45)$$

$$\alpha = 0.138785 \frac{L^2}{t_{1/2}} \quad (46)$$

where $t_{1/2}$ is the time required for the rear face to reach half of its maximum temperature.